CHALMERS

Modelling Stress Relaxation in Bolt Loaded CT–Specimens

Master's Thesis in Nuclear Engineering

SHERVIN SHOJAEE

Department of Applied Physics
Division of Nuclear Engineering
CHALMERS UNIVERSITY OF TECHNOLOGY
Gothenburg, Sweden 2014

Modelling Stress Relaxation in Bolt Loaded CT–Specimens

A Thesis Submitted in Partial Fulfilment of the Requirements for the Degree of Master of Science in Nuclear Engineering

Shervin Shojaee

Department of Applied Physics
Division of Nuclear Engineering
Chalmers University of Technology
Gothenburg, Sweden 2014

Modelling Stress Relaxation in Bolt Loaded CT–Specimens
Master's Degree Thesis in Nuclear Engineering
Shervin Shojaee

Cover:
A bolt loaded CT-specimen.

Modelling Stress Relaxation in Bolt Loaded CT–Specimens
Master's Degree Thesis in Nuclear Engineering
SHERVIN SHOJAEE
Department of Applied Physics
Division of Nuclear Engineering
CHALMERS UNIVERSITY OF TECHNOLOGY

Abstract

Cracks in welds at higher temperature ranges (288 °C) are prone to creep deformation and hence affect the crack tip stresses. Various creep models are presented. One of the models are used to describe the bolt load relaxation of modified CT-specimens analytically. The model is compared to numerical results using Ansys. The long term bolt load relaxation rate described by the model was similar to the three dimensional numerical analysis.

It should be noted that a performed experimental bolt load relaxing experiment was performed, but due to lack of creep deformation data at the temperature of interest, fictive material data parameters were used instead. The CT-specimen was bolt loaded with 16.66 kN. After a 50 h heat treatment cycle at 288 °C, the bolt had relaxed by approximately 30 %.

A bolt load relaxation model for fictive materials were compared with numerical results using the numerical calculation tool Ansys. The shape of the model was consistent with the numerical results, although, some calibrations of the model is still required to reach a satisfying result.

Keywords: CT-specimen, Steady state cracks, Viscoelasticity, Rheology, Creep models, Norton's creep law, Stress relaxation, Stress intensity factor, Numerical analysis.

To my family

Contents

List of Figures

List of Tables

Acknowledgements

Introduction

This report will be introduced with some background information and purpose of the work. It will further be motivated by the reason of its value. The main result of the work lies around a load relaxation model in bolt load modified Compact Tension (CT) specimens[1] which was compared to three dimensional numerical results using Ansys.

Background

Nuclear Power Plants

One of the most essential component in a nuclear power plant (NPP) is the complex piping system. These pipes are exposed to extreme environments in terms of temperature, pressures and chemical interactions. In addition to this, ionising radiation is also present in the most vital parts. The harsh environment make the components prone to development of defects and cracks which eventually leads to fractures if not replaced or repaired. As the safety of a NPP is the highest priority, the understanding of the crack development and crack growth is an essential knowledge of structural integrity of the components.

Crack growth

A substantial portion of the experimental stress corrosion crack growth data for the Swedish nuclear power plant industries have been generated in the autoclaves at Oskarshamn reactor 2 and 3, as well as in hydrogen water chemistry (HWC) and normal water chemistry (NWC) environments. In these experiments, the CT-specimens can be exposed during longer periods of time resulting in an opportunity to model long term behaviours of the stress corrosion cracking. Unfortunately, there are no unambiguous standards to follow for this type of stress corrosion cracking tests regarding the choice of specimens. Considering the standards ASTM E647[2] used for fatigue testing and ASTM E1820[3] used for fracture mechanics testing, the CT-specimen for this experiment seems a reasonable choice.

   With a valid model describing the crack growth over time in these environments, it is possible to foresee when defects reach a critical size. Hence, cyclic inspections can

be established from the models to provide a cost effective and safe maintenance of the reactors.

Generally in fracture mechanics, crack growth follows the Paris law (or some variant of it)[4–6]

$$\frac{da_c}{dN} = A_c(\Delta K)^s,$$

where a_c is the crack length, N the number of load cycles affecting the crack and K the stress intensity factor describing the crack state, which differs for different geometries and loads. As the cyclic loads change from a maximum to a minimum stress intensity factor, ΔK denotes the range of change of the stress intensity factor during the cyclic load. The A_c and s parameters are material dependent.

At most cases, if not always, the avoidance of stress corrosion cracking is the highest priority. The materials' resistance to stress corrosion cracking deviates with dependence on the alloy in use and the environmental influence upon it. Additionally, the structural integrity of any component has to be designed to withstand applied forces, environmental influences, temperature changes and also be economical sustainable in a long term perspective. Nevertheless, stress corrosion cracks in the harsh NPP environments can not be eluded and must therefore be considered when designing a component.

It has been noticed that experimental crack growth data does not meet earlier predictions and it is believed that the creep deformation and stress relaxations influences on the crack front stresses can not be omitted as was earlier assumed reasonable.[7] By making a material creep until the creep behaviour is not longer noticed, the residual stresses can be assumed to be no longer existent (it is most probably the variation of the residual stresses in earlier specimens that gave large variations in the previous measurements). Therefore, it is highly convenient to know for how long a material needs to be exposed to creep deformation until no longer detectable.

Bolt load relaxation experiment

Generally, CT-specimens are applied with active loads in a laboratory environment. Active loads are simply the case when a specie is applied with controlled loads. They are controlled by the tensions of the species, at all times, being adjusted to reach a specific magnitude of force. The testing of this kind is expensive for time consuming experiments, due to the species occupying advanced and expensive equipments. Hence, a modification of the CT-specimens are made for the ability to use passive loads. A passive load is an initially applied load which is not adjusted for the variation over time. In this case, the passive loads are comprised by bolt loading the CT-specimens. The modification was used in an experiment performed by Royal Institute of Technology (KTH) in Sweden. The experiment involved the bolt load relaxation at an elevated temperature[1] (288 °C).

---

1   Elevated temperature relative the room temperature.

Purpose

The work in this report involves the analysis of the collected data from the performed experiment by KTH and to determine whether a valid model of the bolt load relaxation in these environments can be found.

Objective

The project consists of an investigation to determine if there exists analytical models to describe the stress relaxation based on the collected data. As no material data describing the material behaviour could be found, fictional parameters were used and the model were then compared to three dimensional numerical simulations of the specimens.

Scope

Four pre-existing models were investigated. These models are presented. A self derived bolt relaxation model was developed from one of the stress relaxation models and undergoes validation against the numerical simulation of the transient. A finite element method (FEM) model of the CT-specimen is included in the report to demonstrate the stress distribution along the material and to compare the self derived model to numerical results.

The project mainly focuses on the stress relaxation during constant temperature.

Methodology

To understand the models suitability for this kind of problem, a literature study about general fracture mechanics was done. Fracture mechanic is the basic theory and understanding of cracks. Furthermore, various stress relaxation models was searched for, examined, understood and presented. To understand the theories and stress intensities in the CT-specimens with crack defects, a FEM-analysis is included in the report and used for comparison with a self derived stress relaxation model developed from one of the general relaxation models found in literature.

Report structure

This report will handle the basic theories of solid mechanics, cracks and material behaviours in chapter 1. The performed experiment is summarised in chapter 2 along with the stress relaxation models presented. In chapter 3, the numerical set up is explained and the results given. The results are also shown side to side with the theoretical bolt relaxation model. Finally, in chapter 4, various conclusions are made and propositions of future works are given.

List of Abbreviations

Notation	Description
bcc	body centred cubic.
CAD	Computer-Aided Design.
CT	Compact Tension.
fcc	face centred cubic.
FEM	Finite Element Method.
hcp	hexagonal close-packed.
HWC	Hydrogen Water Chemistry.
KTH	The Royal Institute of Technology (Abbreviation of its swedish name; Kungliga Tekniska Högskolan).
L-J	Lennard-Jones.
NPP	Nuclear Power Plant.
NWC	Normal Water Chemistry.
sc	simple cubic.

Notation	Description
SLS	Standard Linear Solid.
TIG	Tungsten Inert Gas.
WEDM	Wire Electric Discharge Machining.

List of Symbols

Notation	Description
A'	Area.
A_c	Paris law parameter.
A	L-J potential parameter or an arbitrary constant in creep equations.
B	L-J potential parameter or CT-specimen thickness.
C	Material parameter describing creep behaviour.
D_0	Material constant for diffusion.
D	Diffusion constant.
E_s, E_d	Activation energy for vacancy movement or formation.
E	Elastic/Young's modulus.
F, F_0	Forces.
F_{initial}	Remaining bolt load after transient.
$F_{\text{remaining}}$	Remaining bolt load after transient.
G	Shear modulus.
H	Height of block.
K_{I}	Stress intensity factor.
K	Stress intensity factor.
L_0	Initial rod length.
N_d	Diffusion constant.

Notation	Description
N	Number of load cycles or number of atoms in a perfect crystal.
P	Force.
Q	Averaged activation energy.
R	Ideal gas constant.
T	Temperature.
V	L-J potential.
W	CT-specimen width.
α	Linear-expansion coefficient.
δ	elongation.
η	Viscosity.
γ	Engineering shear strain.
$\mathbf{D}$	Compliance matrix.
$\mathbf{J}$	Jacobian matrix.
$\mathbf{K}$	Global elemental stiffness matrix.
$\mathbf{L}$	Displacement to strain converting matrix.
$\mathbf{N}$	Shape function matrix.
$\mathbf{U}$	Displacement vector.
$\mathbf{k}$	Elemental stiffness matrix.
ν	Poisson's ratio.
ρ	Radius of curvature.
σ_1	Stress of component 1 in a rheological model.
σ_2	Stress of component 2 in a rheological model.
σ_A	Stress at crack tip.
σ_{tot}	Total stress of the combined components in a rheological model.
σ_∞	Stress applied at the boundary of a large specie.
σ_{YS}	Yield strength.

Notation	Description
σ_{ij}	General notation for stresses. If $i = j$ it denotes tensile stress otherwise it denotes shear stress, in j-direction.
σ	Tensile stress.
τ	Shear stress.
θ	Angle to the crack tip plane.
$\varepsilon, \varepsilon_{\text{axial}}$	Strain. Usually axial/tensile strain.
ε_1	Strain of component 1 in a rheological model.
ε_2	Strain of component 2 in a rheological model.
$\varepsilon_{\text{therm}}$	Thermal strain.
ε_{tot}	Total strain of the combined components in a rheological model.
$\varepsilon_{\text{trans}}$	Transversal strain.
$\vec{J}_{N_d}$	Net flux of a diffusing specie such as vacancies.
$\vec{\sigma}$	Stress vector.
$\vec{\varepsilon}$	Strain vector.
$\vec{d}_e$	Displacement vector of the nodes.
$\vec{d}_g$	Global displacement vector.
$\vec{f}$	Global force vector.
ξ, η	Variables in the parametric coordinate system.
ξ_i, η_i	Node locations expressed in the parametric coordinate system.
a, b	Elliptical geometry parameters describing a potential crack or parameters in a general differential equation. In addition, a could also note the crack length in CT-specimens.
a_{eff}	Effective crack length.
a_c	Crack length.
e	Euler's number.
k_B	Boltzmann's constant.

Notation	Description
k	Characteristic spring constant.
m	L-J potential parameter or material parameter describing creep behaviour.
n	L-J potential parameter, number of vacancies inside a crystal or material parameter describing creep behaviour.
r_0	Atomic separation distance at which they are in equilibrium.
r_y, r_p	Irwin's first and second order plastic zone.
r	Distance to crack tip or atomic separation distance.
s	Paris law parameter.
u_i	Node displacement.
u	Displacement of block with applied shear load or displacement of a point in a coordinate system.
x, y	Variables in the global coordinate system.
x_i, y_i	Node locations expressed in the global coordinate system.

Mechanics of Materials

Mechanics of materials is the knowledge of material behaviour of solids subject to forces. The main goal in this field is to model the deformation of a specific material under various applied loads. This chapter will mainly give a brief overview of central parts, relevant to the subsequent chapters, of mechanical behaviours of materials. The solid material of interest is stainless steel. The chapter will introduce the variables stress and strain as well as concepts such as Hooke's law, elasticity, plasticity, viscoelasticity, creep, stress relaxation and rheological models.

1.1 Material structure

The knowledge of the material structure is the key element of explaining and understanding material behaviours. Crystals are formed by periodic arrays of identical building blocks (eventually, there might be some imperfections or impurities in the crystal structure). One or several atoms act as the building blocks of the formed crystals. The periodic array followed by the building blocks is called lattice.[8]

1.1.1 Atomic structures

The most common lattice configurations are the simple cubic (sc), body-centred cubic (bcc), face-centred cubic (fcc) and the hexagonal close-packed (hcp). These lattice formations, seen in figure 1.1.1, constitute of various planes. Each plane direction is repetitive along the normal-vector of the particular plane. The repetitive planes in a particular direction represents a group of planes. A group of planes have roughly the same bonding strength between every two subsequent planes. The brittleness of a crystal is when it fractures without any extensive deformation. The planes of a material in a brittle crystal is therefore one of the characteristics typically observed. The sodium chloride crystal, NaCl, following a fcc lattice can be seen in figure 1.1.2. The sharp edges are due to the brittle fracture between two subsequent planes.[8]

Crystallites, or grains, are microscopic crystal formations. In the case of most metals, large amount of crystallites are bounded together forming the material, see figure 1.1.3. Solids of this kind are called to be polycrystalline. Pure crystals tend to permanently
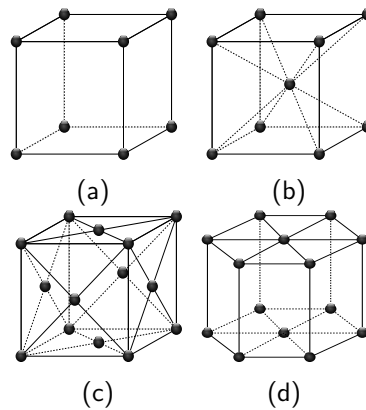
Figure 1.1.1. The lattice structures (a) sc, (b) bcc, (c) fcc and (d) hcp.

Figure 1.1.2.   Magnified picture of a NaCl crystal.   The sharp edges are characteristics shown due to the fcc crystal formation.   (Original source – http://upload.wikimedia.org/wikipedia/commons/8/80/Halite09.jpg)

deform easily, thus have the property of low yield strengths[1] compared to polycrystalline materials.[8] This is mainly due to the variation of orientations in the different grains, preventing the deformation to occur at the grain boundary.

Bondings

There are different types of bondings between atoms, ionic, covalent and metallic. These are considered as primary (strong) bonds. The ionic bonding is when ions pairs up due to their attraction to opposite charges, covalent bonding is when atoms outermost (least energetic orbiting electrons) are shared to a nearby atom and metallic bonding is when electrons are shared as a cloud over several atoms. One type of bondings not mentioned is the secondary type of bonding, long range Van der Waals attraction and close range repulsion. The Lennard-Jones (L-J) potential describes these bondings of

---

[1]   Yield strength is the force, or displacement of atoms, needed to make materials undergo a permanent deformation.
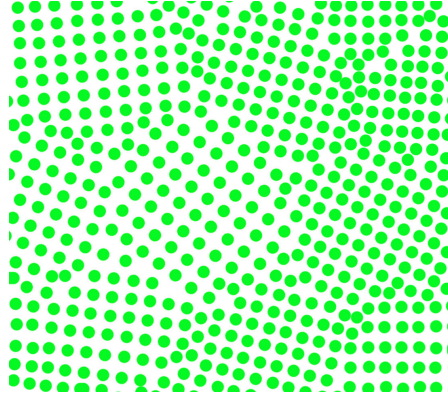
Figure 1.1.3. A polycrystalline lattice formation consists of several crystal structures bounded to each other. The crystal structures, called grains or crystallites, have different orientations relative to each other. (Source – http://upload.wikimedia.org/wikipedia/commons/c/ca/Crystallite.jpg)

spherical atoms (noble gases). Due to the primary bondings also behaving similarly in terms of mathematical description of a potential well in some form, the L-J potential will be used to describe the bondings of metals also, even though not being completely accurate for metallic bonds.[9] A generalised version of the L-J potential is given by

$$V(r) = -\frac{A}{r^n} + \frac{B}{r^m}. \tag{1.1.1}$$

A typical L-J potential with $n = 6$, $m = 12$, $A = 2$ and $B = 1$ can be seen in figure 1.1.4. As earlier mentioned, The L-J potential gives the potential of two interacting atoms where r is the distance between them and A and B some constants describing the amplitude of the attraction and repulsion potential, respectively. It is known from basic physics that $-\frac{dV(r)}{dr} = F(r)$ where $F(r)$ is the force acting on the atoms. Hence,

$$F(r) = -n\frac{A}{r^{n+1}} + m\frac{B}{r^{m+1}}. \tag{1.1.2}$$

The atoms are in equilibrium when the force acting upon them diminish ($F(r_0) = 0$) at a distance r_0. Let equation (1.1.2) be equal to zero to get the distance,

$$F(r_0) = -n\frac{A}{r_0^{n+1}} + m\frac{B}{r_0^{m+1}} = 0 \quad \Longleftrightarrow \quad r_0 = \left(\frac{mB}{nA}\right)^{\frac{1}{m-n}}. \tag{1.1.3}$$

For later use, it should be noted that

$$\left.\frac{dF_0(r)}{dr}\right|_{r=r_0} = \frac{nA}{r_0^{n+2}}(m-n), \tag{1.1.4}$$

where $F_0(r) = -F(r)$ is an external force needed to keep the atoms the distance r apart.
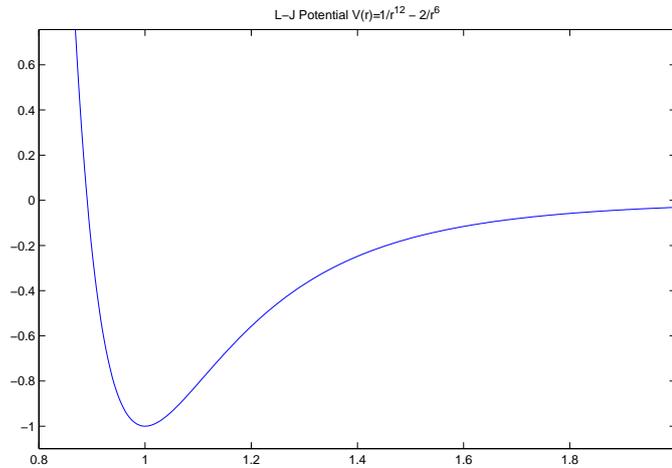
Figure 1.1.4. The L-J potential. Notice the potential minimum describing the distance where the atoms are in rest.
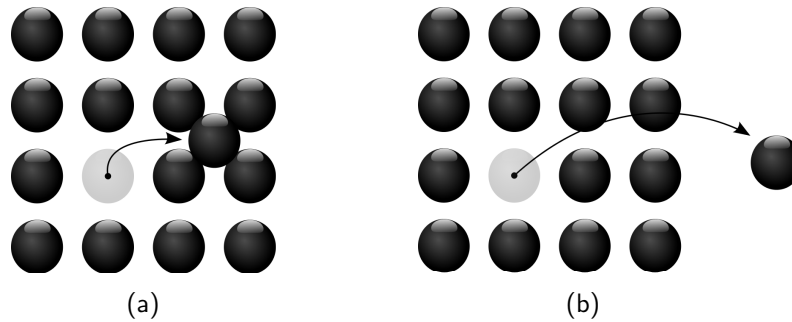
Figure 1.1.5. The (a) Frenkel defect and (b) schottky defect.

Points defects

Point defects such as the well known Schottky defect are common in crystals. The Schottky defect is created in a perfect crystal by removing an atom from a lattice site, creating a vacancy (hole), see figure 1.1.5(b). This process require some energy to take place, E_s. The amount of disorder of the atoms will always be present due to the thermodynamic laws. The probability of a lattice site to have a vacancy is proportional to the Boltzmann factor. Thus, it depending on the energy required to create the vacancy and the temperature in which the crystal is in thermal equilibrium. The number of vacancies n to the number of atoms the perfect crystal would have N is[8]

$$\frac{n}{N-n} = e^{-\frac{E_s}{k_B T}} \tag{1.1.5}$$

where k_B is the Boltzmann constant.

Frenkel defect is an additional variant of point defect. It is recognised by an atom leaving a lattice site and transferred to an interstitial position inside the lattice, see figure

1.1.5(a). The Frenkel defects are not an exception to the thermodynamic laws, hence the number of Frenkel defects are proportional to the Boltzmann factor.[8]

As can be seen by equation (1.1.5), a crystal being formed at higher temperatures give rise to larger number of vacancies. If the crystal is then quenched (suddenly cooled to lower temperatures at a rapid rate) it would still maintain a large amount of the vacancies compared to if the crystal was grown at the quenched temperature. The larger amount of vacancies existing in the crystal than usual will be annihilated by diffusional properties as time goes by. More about diffusion in the section below.

A crystal most often comes with impurities. The impurities are either entirely different atoms than presented by the host crystal or simply a misplaced atom in the host crystal, breaking the periodicity locally. The impurities are occupying the lattice positions inside the crystal. Several important properties, such as mechanical strengthening of materials, arise due to the presence of impurities. Carbon atoms as alloying element are a common addition to iron to produce larger amount of impurities. The carbon atoms will hinder the motion of dislocations, decreasing the weakness and increase the tensile strength of the alloy. The impurities also have the possibility to diffuse inside a material.[8]

Diffusion

With concentration gradients of point defects present inside the material, the defects start to diffuse as a result of the second law of thermodynamics under the constraint that the diffusing specie has sufficient thermal energy to overcome the potential barrier[2] arising from the surroundings. Hence, the diffusion depends on the material temperature and the energy required, called activation energy, to make a transition of the specie from one location inside the crystal to another. The net flux $\vec{J}_{N_d}$ of a particular specie is given by Fick's law[8]

$$\vec{J}_{N_d} = -D\nabla N_d, \tag{1.1.6}$$

where D is the diffusion constant and N_d the concentration of the specie. The diffusion constant is usually expressed as

$$D = D_0 e^{-\frac{E_d}{k_B T}}, \tag{1.1.7}$$

where E_d is the activation energy and D_0 a constant.

Dislocations

Simple theoretical descriptions of the force needed to make a material undergo a permanent deformation are usually overestimations of experimental measurements. In practice, crystals are shown to have lower yield strengths. The deformation of a material is mainly caused by slip of adjacent planes and the lower values are explained due to imperfections inside the crystals in the form of dislocations. An edge dislocation can simply be explained by an insertion of an extra half plane inside the crystal, figure 1.1.6(a). While an edge

---

2   It should be noted that quantum tunnelling is a possible process allowing the diffusion to occur even if the point defect would not have a sufficient thermal energy to bypass the potential barrier.

(a)

(b)
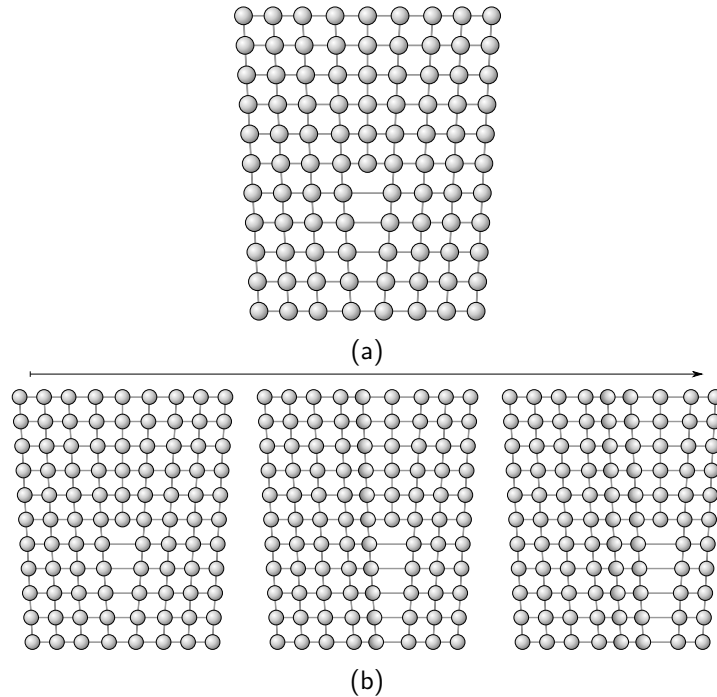
Figure 1.1.6.   The (a) missing plane forming a dislocation in a
lattice and (b) the motion of the dislocation.   (Original source –
https://upload.wikimedia.org/wikipedia/commons/d/dd/Burgers_vektor.svg)

dislocation is present, the stress required to make the slip occur is greatly lowered. This
is due to the possible motion due to the edge dislocations. The motion of dislocations
are illustrated in figure 1.1.6(b). As observed, only parts of the adjacent planes changes
binding locations. Eventually, after several similar steps, the end result will be same as if
the entire adjacent planes being slipped in one step.

1.2   Material behaviour

Consider an uni-axial rod composed of an arbitrary solid material loaded with a force
of magnitude P at both ends with opposite directions, see figure 1.2.1. The material
will, due to the applied force P, be affected by an inner force (with magnitude P) at
an arbitrary cross sectional area A' of the uni-axial rod. The force per unit area, called
stress σ, describes the inner force at each point. If the inner force is evenly distributed at
the cross sectional area, the stress at each point could be described by the mean stress
with respect to the area.[10] Hence,

$$\sigma = \pm \frac{P}{A'} \tag{1.2.1}$$

where minus sign denotes the applied force to be directed towards the rod (compression)
by convention.
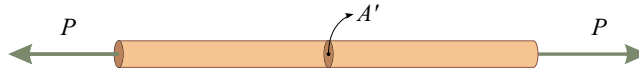
Figure 1.2.1. Applied forces P on a rod with cross-sectional area A'. (Original source – http://upload.wikimedia.org/wikipedia/commons/c/c3/TensionForces.svg)
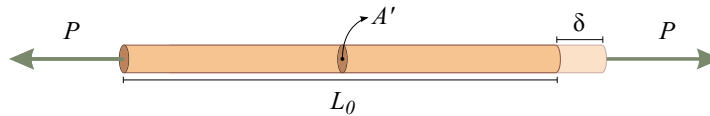
Figure 1.2.2. Applied forces P on a rod with initial length L_0, cross-sectional area A' and the elongation δ. (Original source – http://upload.wikimedia.org/wikipedia/commons/c/c3/TensionForces.svg)

The stress will cause the material to deform. As the applied force (and therefore also the stress) is directed along the axis of the rod, the rod will elongate in that direction, figure 1.2.2. The elongation δ will depend on the initial length L_0 of the rod.[10] The strain ε is given by,

$$\varepsilon = \frac{\delta}{L_0}. \tag{1.2.2}$$

This assumes the deformation to be uniform along the rod. Hence, the strain will be equal to the mean deformation along the rod. The strain gives the percentage of elongation for a infinitesimal volume element, in this case a cylinder with infinitesimal height. The total elongation is therefore the sum of the strain along the rod.

Due to the axial elongation of the rod, it will also undergo a transverse contraction[3] (the diameter of the rod will decrease as the length of it increases). The transverse strain is given by[10]

$$\varepsilon_{\text{trans}} = -\nu\varepsilon_{\text{axial}} \tag{1.2.3}$$

where ν is called the Possion's ratio. For steels and stainless steels $\nu \approx 0.3$.

For other kinds of material geometries or force directions, the applied force P could give rise to an inner force (assume for convenience the inner force to be of same magnitude as the applied force) being parallel to the affected surface A', figure 1.2.3. The force per unit area at each point for this case is called shear stress τ. If the inner force is evenly distributed at the affected area, the shear stress at each point could be described by the mean shear stress with respect to the area.[10] Hence,

$$\tau = \frac{P}{A'}. \tag{1.2.4}$$

A common occurrence is to write a general notation for the shear and tensile stresses as σ_{ij}. The subscript gives the information of the stress being applied in the j–direction

---

[3]   Actually, it exists materials which increases in width as the material is subject to an axial elongation. Although, this is to the rarities and is not the case for steels nor stainless steels.
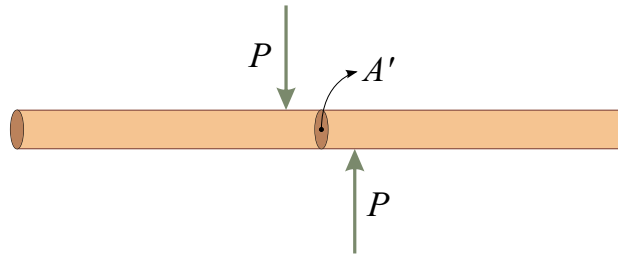
Figure 1.2.3. Applied forces P on a rod with cross-sectional area A'. (Original source – http://upload.wikimedia.org/wikipedia/commons/c/c3/TensionForces.svg)
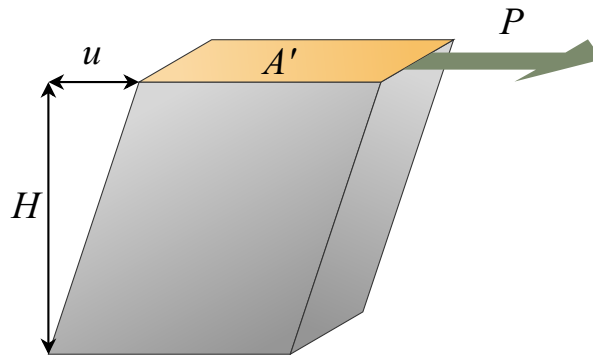
Figure 1.2.4.   Applied forces P on the surface of a rectangular block, with height H and cross-sectional area A', causing a displacement u. (Original source – http://upload.wikimedia.org/wikipedia/commons/d/d0/Shear_scherung.svg)

on a plane with the normal in the i-direction. For $i \neq j$ the stress is simply the shear stress $\sigma_{ij} = \tau_{ij}$. Additionaly, it is known that $\tau_{ij} = \tau_{ji}$ or simply $\sigma_{ij} = \sigma{ji}$.[10]

Consider a rectangular block made of a homogenous material. Applying a shear stress will make it to deform. The deformation, called shear strain and denoted γ, is defined as[10]

$$\gamma = \frac{u}{H}, \tag{1.2.5}$$

where u is the displacement and H the height of the rectangular block, see figure 1.2.4.

It has been experimental verified that a temperature increase could make a material to expand. A thermoelastic material has the property to expand proportional to the temperature change ΔT with the linear-expansion coefficient α (assumed to be constant during the temperature change) as the proportionality factor. The thermoelastic strain is given by[10]

$$\varepsilon_{\text{therm}} = \alpha \Delta T. \tag{1.2.6}$$
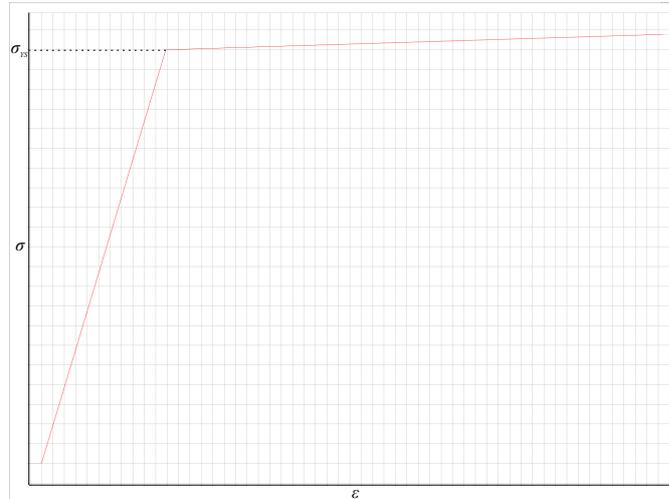
Figure 1.2.5. A bilinear material behaviour with yield stress marked.

1.2.1 Hooke's law and Hooke's generalised law

The properties of a material are experimentally determined. The stress strain relationship for a linear-elastic material is given by Hooke's law[10]

$$\sigma = E\varepsilon \iff \frac{\sigma}{\varepsilon} = \frac{F_0/A'}{\delta/L_0} \approx \frac{dF_0}{dr}\frac{r_0}{A'} = E \tag{1.2.7}$$

where E is the elasticity module for a given material. By inserting equation (1.1.4) into equation (1.2.7), the elasticity module is given by

$$E = \frac{nA}{A'r_0^{n+1}}(m-n). \tag{1.2.8}$$

The material model follow equation (1.2.7) is only valid up to a specified yield strength σ_{YS} for a given material, illustrated for a bilinear constitutive model in figure 1.2.5. A constitutive model is a model of the material behaviour with respect to stress and strain. When the yield strength is reached, a permanent deformation occurs in the material. This kind of instantaneous permanent deformation is called plastic deformation.[1]

Analogously, a simple relationship between shear strain and shear stress is modelled as[10]

$$\tau = G\gamma \tag{1.2.9}$$

where G is the shear modulus of the material.

For isotropic linear-elastic materials in three dimensions, the strains caused by the stresses in each direction and eventually the strain caused by a temperature change, can be superposed. Hence, in a Cartesian coordinate system, the total strain in the x-direction, ε_x, in an infinitesimal volume can be expressed by the stresses σ_x, σ_y and σ_z.

The partial strains occurring due to the stresses in the x, y and z-direction are denoted ε_{x1}, ε_{x2} and ε_{x3}, respectively. Equation (1.2.3) and equation (1.2.7) gives

$$\varepsilon_{x1} = \frac{\sigma_x}{E} \tag{1.2.10}$$

$$\varepsilon_{x2} = -\nu\frac{\sigma_y}{E} \tag{1.2.11}$$

$$\varepsilon_{x3} = -\nu\frac{\sigma_z}{E}. \tag{1.2.12}$$

By considering the thermoelastic properties of the material with the strain-temperature relationship given by equation (1.2.6), the total strain in the x-direction (and analogously, the total strain in the y and z-direction) is given by

$$\varepsilon_x = \frac{1}{E}\big(\sigma_x - \nu(\sigma_y + \sigma_z)\big) + \alpha\Delta T \tag{1.2.13}$$

$$\varepsilon_y = \frac{1}{E}\big(\sigma_y - \nu(\sigma_x + \sigma_z)\big) + \alpha\Delta T \tag{1.2.14}$$

$$\varepsilon_z = \frac{1}{E}\big(\sigma_z - \nu(\sigma_x + \sigma_y)\big) + \alpha\Delta T. \tag{1.2.15}$$

Recalling equation (1.2.9), the possible shear strains acting upon the infinitesimal volume are

$$\gamma_{xy} = \frac{\tau_{xy}}{G} \tag{1.2.16}$$

$$\gamma_{yz} = \frac{\tau_{yz}}{G} \tag{1.2.17}$$

$$\gamma_{zx} = \frac{\tau_{zx}}{G}. \tag{1.2.18}$$

Equation (1.2.13) to equation (1.2.18) gives the stress-strain relationship for an isotropic linear-elastic material. They are called Hooke's generalised law. [10]

Plane stress and plane strain

An important special case of Hooke's generalised law is when stresses in one of the directions are zero, for example when $\sigma_z = \gamma_{yz} = \gamma_{zx} = 0$. Whence,

$$\varepsilon_x = \frac{1}{E}(\sigma_x - \nu\sigma_y) + \alpha\Delta T \tag{1.2.19}$$

$$\varepsilon_y = \frac{1}{E}(\sigma_y - \nu\sigma_x) + \alpha\Delta T \tag{1.2.20}$$

$$\varepsilon_z = -\frac{\nu}{E}(\sigma_x + \sigma_y) + \alpha\Delta T \tag{1.2.21}$$

$$\gamma_{xy} = \frac{\tau_{xy}}{G}. \tag{1.2.22}$$

This practical case is commonly known as a material being under plane stress, hence giving Hooke's generalised law of plane stress. [10]

Similarly, there could arise cases when there are no strains in one of the directions. Let $\varepsilon_z = \gamma_{yz} = \gamma_{zx} = 0$ and Hooke's generalised law could be written as

$$\varepsilon_x = \frac{1 - \nu^2}{E}\left(\sigma_x - \frac{\nu}{1 - \nu}\sigma_y\right) + (1 + \nu)\alpha\Delta T \tag{1.2.23}$$

$$\varepsilon_y = \frac{1 - \nu^2}{E}\left(\sigma_y - \frac{\nu}{1 - \nu}\sigma_x\right) + (1 + \nu)\alpha\Delta T \tag{1.2.24}$$

$$\gamma_{xy} = \frac{2\tau_{xy}(1 + \nu)}{E}. \tag{1.2.25}$$

which is called Hooke's generalised law for plane deformation. [10]

1.2.2 Elasticity, plasticity and viscoelasticity

The word *elastic* has been mentioned several times in §1.2 as well as in §1.2.1. It is used to describe a material property. If a material is able to return to its original shape and size when an applied stress (or increased temperature) has been removed, it is called to have elastic properties. [10] The elasticity of the material could be linear, as have been assumed by Hooke's law §1.2.1, or non-linear. Almost all metals and alloys exhibits elastic properties for small strains/stresses at room temperature. Unfortunately, the nessecity of other complicated models could be required. This is usually due to materials being exposed to environments with increased temperature and/or being under a larger strain. [6]

When forces applied to an object invokes sufficiently large internal stresses, the material will have an inelastic behaviour. This will in general lead to permanent deformations in the material. Thus, the deformations will be maintained even when the material no longer are subject to any forces. The material is called to have a *plastic* behaviour during the deformation. [10]

Viscoelasticity is a material property which obeys both viscous and elastic conditions. The viscous properties of materials is the ability to resist strain linearly when a stress is applied in a point. Thus, a viscoelastic property is the material's instant deformation due to (time-independent) elasticity and a time-dependent deformation due to the viscous property. [6]

There is also a definition for *viscoplasticity*. Remarking that viscoplastic creep (more about creep in §1.2.3) is a special case of a viscoelastic material behaviour. [1]

Linear and non-linear viscoelastic materials

Linear viscoelastic materials are defined as the case when the elasticity and viscosity are linear. The elasticity of the material follows Hooke's law, equation (1.2.7). The linear viscosity is defined by the deformation rate being proportional to the stress [10]

$$\frac{d\varepsilon}{dt} = \frac{\sigma}{\eta}, \tag{1.2.26}$$

where η is the viscosity of the material. As an example, a simple linear viscoelastic material behaviour could be the sum of equation (1.2.26) and the time-derivative of equation (1.2.7)

$$\frac{d\varepsilon}{dt} = \frac{1}{E}\frac{d\sigma}{dt} + \frac{\sigma}{\eta}. \tag{1.2.27}$$

A simple model of a non-linear viscoelastic material can be given by the sum of the time-derivative of Hooke's law given by equation (1.2.7) and

$$\frac{d\varepsilon}{dt} = A\sigma^n, \tag{1.2.28}$$

where A is an arbitrary constant and n a non-linearity material behaviour parameter. The power dependence of the strain-rate represents the non-linearity in the viscous model shown in equation (1.2.28). The simple non-linear viscoelastic model is thus given by

$$\frac{d\varepsilon}{dt} = \frac{1}{E}\frac{d\sigma}{dt} + A\sigma^n. \tag{1.2.29}$$

1.2.3 Creep deformation

Diffusional flow and dislocation motion inside a material causes the material to deform with time (often modelled as viscosity, see §1.2.2 and §2.2). The vacancies and dislocations are strongly temperature and stress dependent. The time-dependent deformation is called creep. Creep is said to be of importance in metals only when above approximately 30 % to 60 % of its absolute melting point. [6]

It has been experimentally observed that the creep deformation with time follows three states under constant stress, [6]

1. *Primary (transient):* An initially large strain-rate is decreasing over time. The strain-rate is decreasing due to strain-hardening[4].

2. *Secondary (steady-state):* A constant strain-rate is maintained.

3. *Tertiary (unstable):* The material suddenly loses strength and the strain-rate increases until the material ruptures.

A graph of the sequence of events can be seen in figure 1.2.6.

From the physics behind different states in a crystal lattice (explained in §1.1.1) it is expected to believe that the deformation caused by the diffusion of vacancies and dislocation motions to be proportional to Boltzmann's distribution. Averaging over the energy states give instead that the strain-rate is given by Arrhenius equation [6]

$$\frac{d\varepsilon}{dt} = A_0 e^{-\frac{Q}{RT}}, \tag{1.2.30}$$

---

[4] The material is hardening due to an increased amount of dislocations during the initial deformation phase.
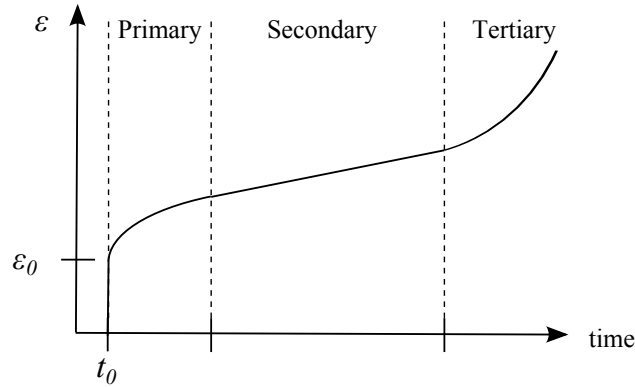
Figure 1.2.6.   A typical creep behaviour and the name of its different states.   The constants ε_0 and t_0 denotes the initial strain and the time at which creep starts to occur, respectively.   (Original source – http://upload.wikimedia.org/wikipedia/commons/4/4d/3StageCreep.svg)

with Q being the activation energy for a change or particle/molecule motion inside the medium. The parameter T is the absolute temperature of the material and R is the universal gas constant. The constant A_0 depends on stress, average grain diameter and temperature. Assuming the temperature and average grain diameter to be constant over time and that the strain rate is proportional to a power of the applied stress, the general equation for steady-state creep rate is given as[6]

$$\frac{d\varepsilon}{dt} = C\sigma^m e^{-\frac{Q}{RT}}, \tag{1.2.31}$$

where C is a constant that depends on temperature and average grain diameter. Equation (1.2.31) gives either a linear or non-linear viscous property depending on the value of m. The reason for equation (1.2.31) to be valid only for steady-state creep is due to the assumption that no change in amount of dislocations or impurities occurs but rather held constant, only the motion of them are considered. Further assuming a constant activation energy Q equation (1.2.31) simply leads to equation (1.2.28).

1.2.4   Stress relaxation

As creep is defined as the time-dependent deformation of a material under stress, a stress relaxation is the stress change of a material over time when kept under constant strain.[6] It has been shown that the stress relaxes, that is, the stress required to keep a material under constant strain is decreasing over time. This relaxation is due to impurities and dislocations concentrations to reach a homogenisation throughout the material and/or in ductile materials due to increased amount of voids, making the material weaker. With a constitutive model for the material behaviour, simply this means to find an expression for σ when

$$\frac{d\varepsilon_{\text{tot}}}{dt} = 0, \tag{1.2.32}$$

where ε_{tot} is the total strain.

1.3 Cracks

When the bondings in the lattice of an individual grain are too weak to withstand the external forces being applied, it will break apart. The fracture of this kind is called to be a transgranular fracture. The opposite of a transgranular fracture is the intergranular fracture. The intergranular fracture is when the bondings between two grains (the grain boundary) is broken.

1.3.1 Stresses near a crack tip

Assuming to have an elliptical shaped (with the large axis a and short axis b) crack inside a large specie with a stress σ_∞ applied at the boundary as being shown in figure 1.3.1. The stress σ_A at the tip of the crack (point A) will be given by[1]

$$\sigma_A = \sigma_\infty \left(1 + \frac{2a}{b} \right). \tag{1.3.1}$$

The stress concentration factor k_t is defined as the ratio $\frac{\sigma_A}{\sigma_\infty}$ in this particular case. Let $a = b$, hence the crack having the shape of a circular hole, gives $k_t = 3$ which is a well known result.[1]

Now instead let $a \gg b$. The ellipse will have a sharp crack shape. For such a case equation (1.3.1) is instead expressed by the radius of curvature $\rho = \frac{b^2}{a}$ at the tip of the crack

$$\sigma_A = \sigma_\infty \left(1 + 2\sqrt{\frac{a}{\rho}} \right). \tag{1.3.2}$$

Because $a \gg b$, equation (1.3.2) can be written as

$$\sigma_A = 2\sigma_\infty \sqrt{\frac{a}{\rho}}. \tag{1.3.3}$$

The smallest size of the radius of curvature in real life will be in order of an atomic radius. Equation (1.3.3) is valid for brittle materials. Due to metals deforming plastically, an initially infinitely sharp crack will blunt. Thus, the metals will have slightly lower crack tip stress depending on the order of the crack tip blunt.

There are specific geometries and crack configurations where the possibility of deriving expressions for the stresses inside the body exists. Figure 1.3.2 illustrates the stresses in an infinitesimal volume near the crack tip. It has been shown that the stress in any linear elastic isotropic cracked body could be expressed as[1]

$$\sigma_{ij} = \left(\frac{k}{\sqrt{r}} \right) f_{ij}(\theta) + \sum_{m=0}^{\infty} A_m r^{\frac{m}{2}} g_{ij}^{(m)}(\theta), \tag{1.3.4}$$
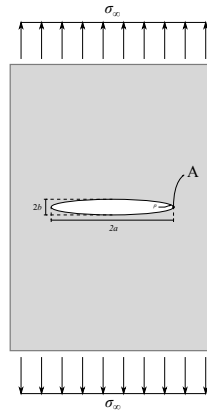
Figure 1.3.1. Applied stresses at the boundary of a large specie with an elliptical shaped crack in the centre.
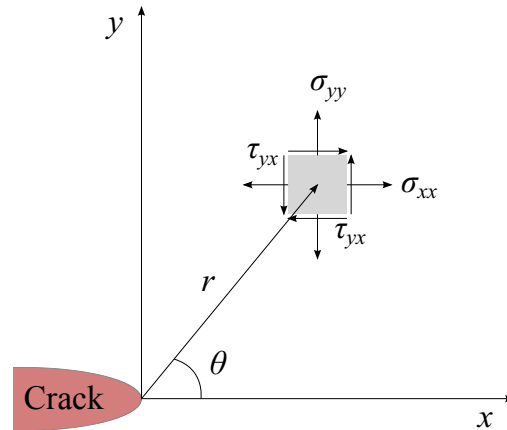
Figure 1.3.2. The stresses in an infinitesimal volume near the crack tip.

where r is the distance from the crack tip, θ the angle to the crack tip plane and k a proportionality constant. Note that the leading term in equation (1.3.4) when $r \ll 1$ is

$$\sigma_{ij} \approx \frac{k}{\sqrt{r}} f_{ij}(\theta). \tag{1.3.5}$$

Hence, it has been shown that the stress close to the crack tip varies with $\frac{1}{\sqrt{r}}$.

1.3.2   Loading modes

There are three categorised cases for which the crack is subject to stresses. The categorised cases, called modes, are denoted with the sub– and superscripts I, II and III. The three different loading modes can be seen in figure 1.3.3. As k and $f_{ij}(\theta)$ in equation (1.3.5)
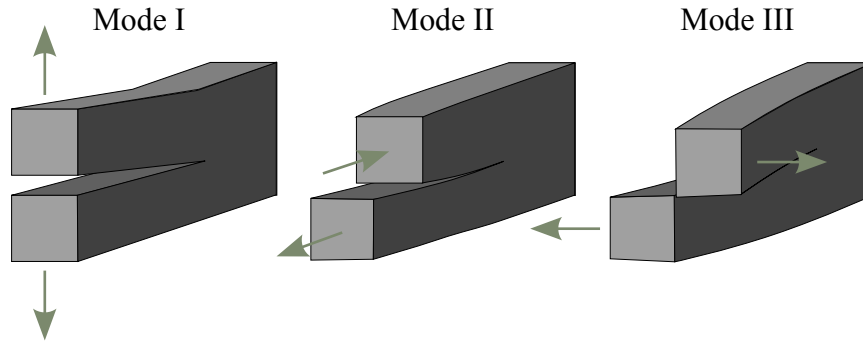
Figure 1.3.3.   The three different loading modes.   (Original source –
http://upload.wikimedia.org/wikipedia/commons/e/e7/Fracture_modes_v2.svg)

depends on the loading mode, they are rewritten with the corresponding subscripts for
the particular loading case. Mode I will be the only mode considered here. Defining the
stress intensity factor for mode I as $K_\mathrm{I} = k_\mathrm{I}\sqrt{2\pi}$ and recalling equation (1.3.5) gives

$$\sigma_{ij}^{(\mathrm{I})} \approx \frac{K_\mathrm{I}}{\sqrt{2\pi r}} f_{ij}^{(\mathrm{I})}(\theta), \quad r \ll 1. \tag{1.3.6}$$

The functions $f_{ij}^{(\mathrm{I})}(\theta)$ with $i, j \in \{x, y, z\}$ are given in table 1.3.1.[1] The region where
equation (1.3.6) is valid is called the singularity dominated zone, see figure 1.3.4. In §1.2
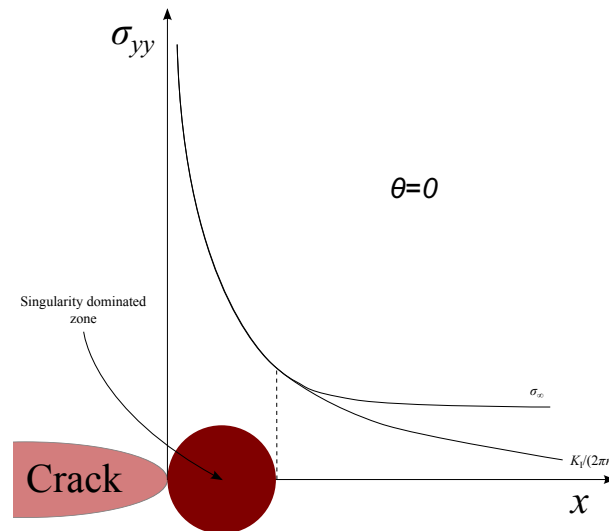
Figure 1.3.4. The stresses and distance near the crack tip (close to the singularity
dominated zone) are inversely proportional to the stress intensity factor.

it has been mentioned that $\sigma_{ij} = \sigma_{ji}$ and therefore it follows that $f_{ij}^{(\mathrm{I})} = f_{ji}^{(\mathrm{I})}$. Considering
table 1.3.1 and equation (1.3.6), the tensile stress components σ_{xx} and σ_{yy} at the crack

Table 1.3.1. The functions $f_{ij}^{(\mathrm{I})}$ for $i, j \in \{x, y, z\}$.

$f_{xx}^{(\mathrm{I})}(\theta)$	$\cos\frac{\theta}{2}\left(1 - \sin\frac{\theta}{2}\sin\frac{3\theta}{2}\right)$
$f_{yy}^{(\mathrm{I})}(\theta)$	$\cos\frac{\theta}{2}\left(1 + \sin\frac{\theta}{2}\sin\frac{3\theta}{2}\right)$
$f_{xy}^{(\mathrm{I})}(\theta)$	$\cos\frac{\theta}{2}\sin\frac{\theta}{2}\cos\frac{3\theta}{2}$
$f_{zz}^{(\mathrm{I})}(\theta)$	0 (Plain stress) $2\nu\cos\frac{\theta}{2}$ (Plane strain)

plane ($\theta = 0$) near the crack tip is given by

$$\sigma_{xx} = \sigma_{yy} = \frac{K_{\mathrm{I}}}{\sqrt{2\pi r}}. \tag{1.3.7}$$

The stress intensity factor describes the state of the crack. It depends, in addition to the loading mode, on the shape of the crack tip and the geometry of the the cracked body. For a CT specimen in mode I load the stress intensity factor is given by[1,5]

$$K_{\mathrm{I}}(a) = \frac{P}{B\sqrt{W}}\frac{2 + \frac{a}{W}}{\left(1 - \frac{a}{W}\right)^{\frac{3}{4}}}\left(0.886 + 4.64\left(\frac{a}{W}\right) - 13.32\left(\frac{a}{W}\right)^2\right.$$
$$\left. + 14.72\left(\frac{a}{W}\right)^3 - 5.60\left(\frac{a}{W}\right)^4\right), \tag{1.3.8}$$

where W is the width of the specimen, a the crack length, P the applied force and B the thickness. The standardised CT-specimen with the dimensions are shown in figure 1.3.5. Please note that $0.2W$ is the distance from the centre of holes to the notch edge and a is the distance from the centre of holes to the crack edge.

1.3.3 Irwin plastic correction approach

Due to the crack tip plasticity, an approximation is made to overcome the plastic effects. In linear elastic fracture mechanics the Irwin approach is one of the methods to accomplish this.

At the crack plane in a CT specimen, the yielding occur when $\sigma yy = \sigma_{\mathrm{YS}}$. Substituting σ_{YS} into equation (1.3.7) give the so called first order estimate of the plastic zone for plane stress[1]

$$r_y = \frac{1}{2\pi}\left(\frac{K_{\mathrm{I}}}{\sigma_{\mathrm{YS}}}\right)^2. \tag{1.3.9}$$

By neglecting the strain hardening effects in the plastic region, the stress is given by $\sigma_{yy} = \sigma_{\mathrm{YS}}$ for $r < r_y$. This will underestimate the sum of the stresses in front of the
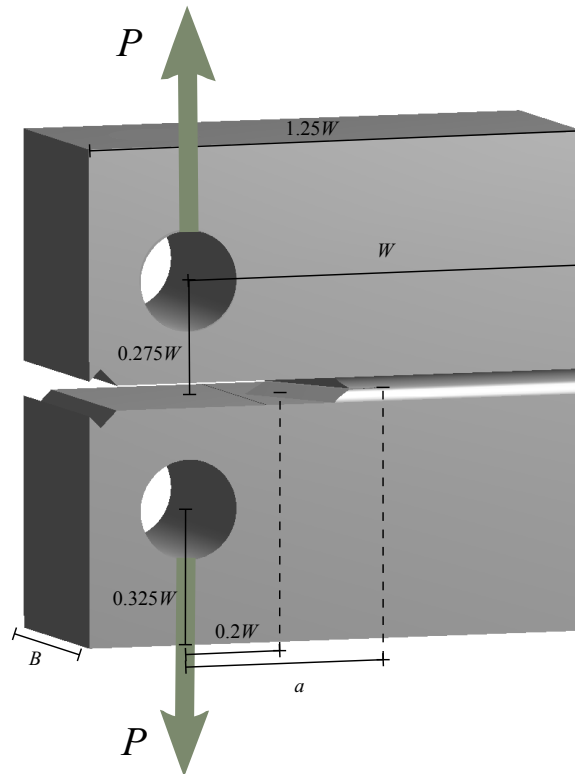
Figure 1.3.5. The standardised CT-specimen with dimensions.

crack tip. The second order estimate of the plastic zone r_p takes care of this by a simple force balance. It is given to be twice the size of the first order estimated plastic zone[1]

$$r_p = 2r_y. \tag{1.3.10}$$

This method redistributes the stresses. The stresses in the elastic region (the region outside the plastic zones) will be larger and must be taken into account. The larger stresses implies that the state of the crack is different, hence the stress intensity factor needs to be modified. It has been realised that when assuming the crack size to be a_{eff} where

$$a_{\text{eff}} = a + r_y, \tag{1.3.11}$$

yields a good approximation to the new stress intensity factor $K_{\text{I}_{\text{eff}}} = K_{\text{I}}(a_{\text{eff}})$. This process could be iterated four or five times if needed. That is, with $K_{\text{I}_{\text{eff}}}$, find new estimations of the plastic zones with equation (1.3.9) which in turn is used to define the new virtual crack length with equation (1.3.11) and so forth. A schematic map of the iteration is shown in figure 1.3.6.
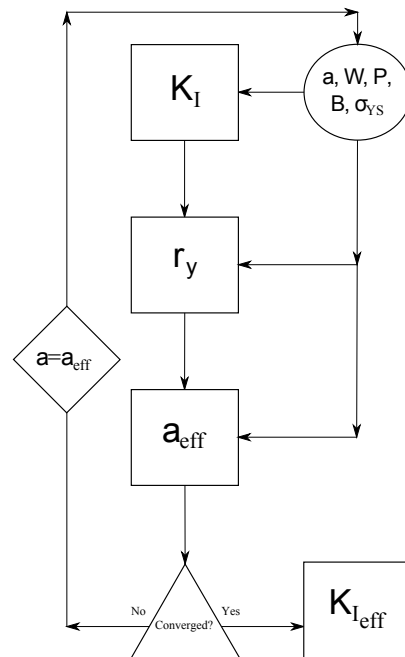
Figure 1.3.6. A schematic figure of Irwin iteration process.

1.4   Numerical computational calculations

Ever since the development of computational numerical modelling, it has been considered an important tool for practical problems without closed-formed solutions. Fortunately, the computational power has increased and substantially less time is required to find a suitable solution due to more efficient algorithms, compared to the situation a decade ago. This makes the numerical analysis even more tempting to be used for various problems.[1] Various numerical algorithms and techniques have been developed and applied to solid mechanics. The commonly known are the finite difference[11], finite element[12] and boundary integral equation methods[13]. Currently, FEM is by far the most common analysis method utilised for cracked bodies and will be briefly explained.

1.4.1   Finite element method

With FEM, the geometry to calculate stresses and displacements in each point, is subdivided into discrete shapes called *elements*. The procedure of creating elements in a body is called *meshing*. The elements, which could be made of one-dimensional beams, two-dimensional plane stress or plane strain and three dimensional bricks, are connected at *nodes* where continuity of displacement constraints are applied. Consider a two-dimensional element, figure 1.4.1, with parametric and global coordinates ξ-η and x-y, respectively. In the parametric coordinate system, all points (ξ, η) inside the element are given by $\xi, \eta \in [-1, 1]$. In the global coordinate system, the same points inside the
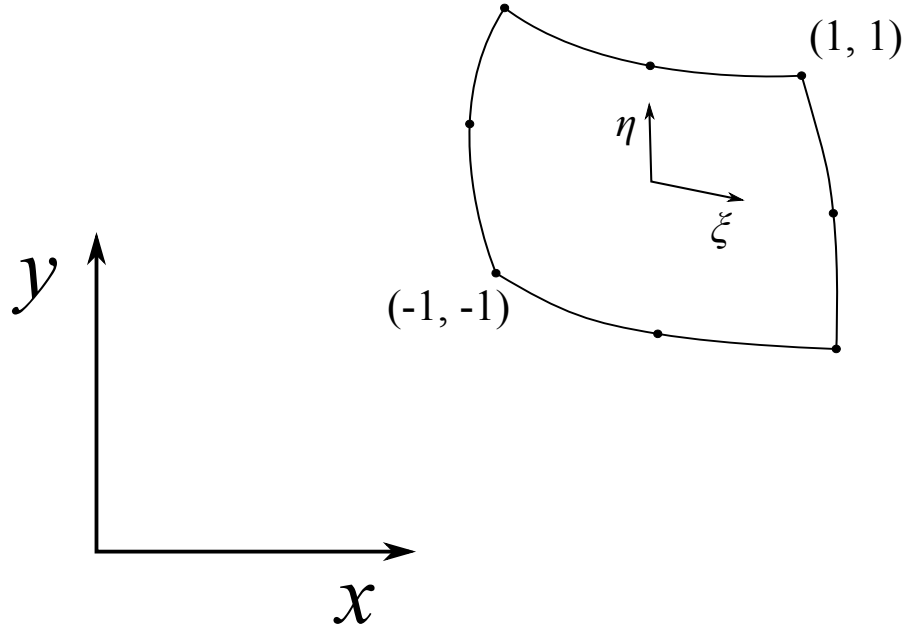
Figure 1.4.1. A two-dimensional element with 8 nodes together with parametric and global coordinates.

element are given by [1]

$$x = \sum_{i=1}^{n} N_i(\xi,\eta) x_i \qquad (1.4.1)$$

for the x-direction, and

$$y = \sum_{i=1}^{n} N_i(\xi,\eta) y_i \qquad (1.4.2)$$

for the y-direction. Here, n is the number of nodes in the element and N_i are shape functions corresponding to node i. The x_i and y_i variables are the node locations in the global coordinate system for node i. Please note that all points inside the element is described by the position of the nodes and the shape functions.

The shape functions are polynomials whose degree depend on the number of nodes in the element. For a two-dimensional element with four nodes (one at each at the corner), figure 1.4.2(a), the shape functions are linear while consisting of 8 nodes, as shown in figure 1.4.2(b), they are quadratic. The quadratic interpolation shape functions are given by

$$N_i(\xi,\eta) = \left((1 + \xi\xi_i)(1 + \eta\eta_i) - (1 - \xi^2)(1 + \eta\eta_i) - (1 - \eta^2)(1 + \xi\xi_i)\right)\frac{\xi_i^2 \eta_i^2}{4}$$

$$+ (1 - \xi^2)(1 + \eta\eta_i)(1 - \xi_i^2)\frac{\eta_i^2}{2} + (1 - \eta^2)(1 + \xi\xi_i)(1 - \eta_i^2)\frac{\xi_i^2}{2}, \quad (1.4.3)$$
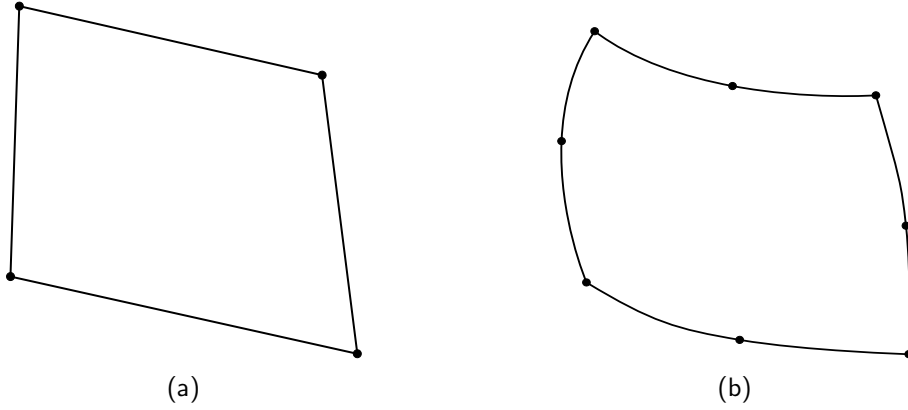
Figure 1.4.2. A two-dimensional (a) 4 node element and (b) 8 node element.

where ξ_i and η_i are the coordinates of node i in the parametric coordinate system, where $(\xi_i, \eta_i) \in \left\{(\Xi, \Psi) \in \{-1, 0, 1\}^2 : \Xi \neq 0 \vee \Psi \neq 0\right\}$. The displacements within the element are expressed as

$$u = \sum_{i=1}^{n} N_i(\xi,\eta)u_i \qquad (1.4.4)$$

$$v = \sum_{i=1}^{n} N_i(\xi,\eta)v_i, \qquad (1.4.5)$$

where (u_i, v_i) is the displacement for node i in the x- and y-direction, respectively. The displacements describe the change in position of each point inside an element and thus depends on the change in position of the nodes. The equation system given by equation (1.4.4) and equation (1.4.5) can be written as

$$\mathbf{U} = \mathbf{N}\vec{d_e}, \qquad (1.4.6)$$

where

$$\mathbf{U} = \begin{pmatrix} u \\ v \end{pmatrix}, \quad \mathbf{N} = \begin{pmatrix} N_1 & 0 & N_2 & 0 & \cdots & N_n & 0 \\ 0 & N_1 & 0 & N_2 & \cdots & 0 & N_n \end{pmatrix}, \quad \vec{d_e} = \begin{pmatrix} u_1 \\ v_1 \\ u_2 \\ v_2 \\ \vdots \\ u_n \\ v_n \end{pmatrix}.$$

The strain vector $\vec{\varepsilon}$ is given by [1]

$$\vec{\varepsilon} = \mathbf{L}\mathbf{U} \qquad (1.4.7)$$

with

$$
\vec{\varepsilon} = \begin{pmatrix} \varepsilon_x \\ \varepsilon_y \\ \gamma_{xy} \end{pmatrix}, \quad \mathbf{L} = \begin{pmatrix} \frac{\partial}{\partial x} & 0 \\ 0 & \frac{\partial}{\partial y} \\ \frac{\partial}{\partial y} & \frac{\partial}{\partial x} \end{pmatrix}.
$$

Equation (1.4.6) and equation (1.4.7) gives

$$
\vec{\varepsilon} = \mathbf{L}\mathbf{N}\vec{d_e} = \mathbf{B}\vec{d_e}, \tag{1.4.8}
$$

where

$$
\mathbf{L}\mathbf{N} = \mathbf{B} = \begin{pmatrix} \frac{\partial N_1}{\partial x} & 0 & \frac{\partial N_2}{\partial x} & 0 & \cdots & \frac{\partial N_n}{\partial x} & 0 \\ 0 & \frac{\partial N_1}{\partial y} & 0 & \frac{\partial N_2}{\partial y} & \cdots & 0 & \frac{\partial N_n}{\partial y} \\ \frac{\partial N_1}{\partial y} & \frac{\partial N_1}{\partial x} & \frac{\partial N_2}{\partial y} & \frac{\partial N_2}{\partial x} & \cdots & \frac{\partial N_n}{\partial y} & \frac{\partial N_n}{\partial x} \end{pmatrix}.
$$

The shape functions, expressed by equation (1.4.3), are given as functions with variables in the parametric coordinate-system (ξ and η). Their derivatives with respect to the variables in the global coordinate-system (x and y), as expressed in $\mathbf{B}$, are found with the help of the Jacobian matrix $\mathbf{J}$ by the relation

$$
\begin{pmatrix} \frac{\partial N_1}{\partial x} & \frac{\partial N_2}{\partial x} & \cdots & \frac{\partial N_n}{\partial x} \\ \frac{\partial N_1}{\partial y} & \frac{\partial N_2}{\partial y} & \cdots & \frac{\partial N_n}{\partial y} \end{pmatrix} = \mathbf{J}^{-1} \begin{pmatrix} \frac{\partial N_1}{\partial \xi} & \frac{\partial N_2}{\partial \xi} & \cdots & \frac{\partial N_n}{\partial \xi} \\ \frac{\partial N_1}{\partial \eta} & \frac{\partial N_2}{\partial \eta} & \cdots & \frac{\partial N_n}{\partial \eta} \end{pmatrix}. \tag{1.4.9}
$$

The Jacobian is given by

$$
\mathbf{J} = \begin{pmatrix} \frac{\partial x}{\partial \xi} & \frac{\partial y}{\partial \xi} \\ \frac{\partial x}{\partial \eta} & \frac{\partial y}{\partial \eta} \end{pmatrix} = \begin{pmatrix} \frac{\partial N_1}{\partial \xi} & \frac{\partial N_2}{\partial \xi} & \cdots & \frac{\partial N_n}{\partial \xi} \\ \frac{\partial N_1}{\partial \eta} & \frac{\partial N_2}{\partial \eta} & \cdots & \frac{\partial N_n}{\partial \eta} \end{pmatrix} \begin{pmatrix} x_1 & y_1 \\ x_2 & y_2 \\ \vdots & \vdots \\ x_n & y_n \end{pmatrix} \tag{1.4.10}
$$

where the last equality is gotten by considering equation (1.4.1) and equation (1.4.2).

As the strain vector $\vec{\varepsilon}$ is known, the stress vector can be calculated by

$$
\vec{\sigma} = \mathbf{D}^{-1}\vec{\varepsilon} \tag{1.4.11}
$$

where $\mathbf{D}$ is the compliance matrix for the given material, which could be given by Hooke's generalised law in two dimensions. For a material that has a varying compliance matrix as the stress and/or strain incrementally change, the compliance matrix is updated each load step

$$
\Delta\vec{\sigma} = \mathbf{D}^{-1}\Delta\vec{\varepsilon}. \tag{1.4.12}
$$

To find the stresses and strains in each element, the displacements of all the nodes has to be known. The displacements depend on the elemental stiffness matrix $\mathbf{k}$ given by

$$
\mathbf{k} = \int_{-1}^{1} \int_{-1}^{1} \mathbf{B}^{\top}\mathbf{D}\mathbf{B}|\det \mathbf{J}|d\xi d\eta. \tag{1.4.13}
$$
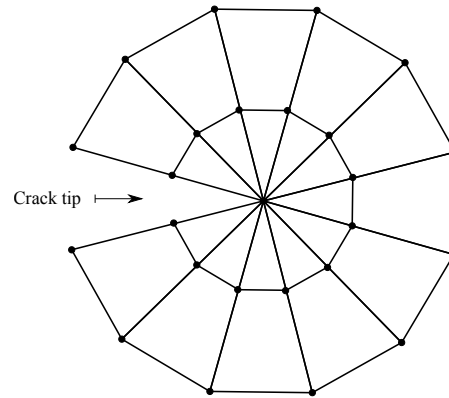
Figure 1.4.3. The mesh around the crack tip. This mesh design yields a mathematical $\frac{1}{\sqrt{r}}$ singularity behaviour in front of the defect.

All individual elemental stiffness matrices are expanded and summed to get the global elemental stiffness matrix $\mathbf{K}$, which won't be explained further in this report. The global force $\vec{f}$ and displacement vectors $\vec{d_g}$ of all the nodes are related as follows

$$\mathbf{K}\vec{d_g} = \vec{f}. \tag{1.4.14}$$

Crack tip mesh design

To reduce the calculation time, a reduction of elements are beneficial. To reduce number of elements without losing accuracy, a clever strategy has to be considered.

In a cracked body, the elements in front of the crack tip can be designed in such a way to get a $\frac{1}{\sqrt{r}}$ singularity as expressed in equation (1.3.5). This would give a better numerical accuracy, with less number of elements.[1] The design is simply a degeneration of quadrilateral elements into triangles at the crack tip, as shown in figure 1.4.3.

2 Chapter

The knowledge of anything, since all things have causes, is not acquired or complete unless it is known by its causes.

– Pur-e Sina

Methodology

By using the results of an already performed experiment (described in §2.1), they are compared to one of the stress relaxation models given in §2.2. The parameters of the creep models were to be obtained by the use of uniaxial creep experiment results but due to lack of uniaxial creep experiments, fictive parameters were used. These parameters were then used to simulate the experimental transient in a numerical calculation tool called Ansys (see §3.1).

2.1 Experiment

The experimental procedure contained several steps. Swerea KIMAB has manufactured the CT-specimens. The specimens were delivered to KTH in Sweden. At KTH, the specimens were modified for the possibility of bolt loading, crack initiation and heat treatment for stress relaxation under fixed load.

2.1.1 Manufacturing the CT-specimens

Test blocks were manufactured by milling round bars with diameter of $130\,\mathrm{mm}$ to square bars. A U-shaped joint was made according to drawing 1090900 Revision 03 given in appendix B. The U-joints were filled using Tungsten Inert Gas (TIG) welding[14] with the filler metal Avesta 308LSi. After the welding procedure, the test blocks were cut by $25\,\mathrm{mm}$ from each side to remove impurities often located near the surfaces. If visible defects was observed after the cutting, the test block was cut further until a defect-free block was obtained. The test blocks was thereafter processed into CT-specimens with the dimensions according to the drawing 3003329 Revision 2 shown in appendix A. At KTH's Solid Mechanics department the notch of the specimen was processed using wire electric discharge machining (WEDM). Side grooves was also processed in the specimen. The specimens was further modified by drilling a hole with an internal thread to fit a M12 bolt.[15]

2.1.2   Crack initiation

A material testing system equipment was a necessity to induce cyclic loading on the specimens. By the use of the equipments MTS 100 kN 1.3 and 1.4, this was accomplished to initiate a sharp crack. The load was measured with the built-in load sensors and the crack mouth opening displacement with a clip gauge, Instron model 2670. The maximal load of the cycle was in such order that $K_{I_{max}} = 18\,\mathrm{MPam}^{1/2}$ which was gradually lowered until reaching approximately $16\,\mathrm{MPam}^{1/2}$. This procedure ended up with a crack of $a = 25\,\mathrm{mm}$ in size (see figure 1.3.5).

2.1.3   Bolt loading

With MTS 100 kN 1.3 and Instron model 2670, the specimen was loaded until the stress intensity factor $K_I \approx 30\,\mathrm{MPam}^{1/2}$ was obtained. At the tensioning, some creep effects was detected by the clip gauge. The loading was adjusted during the creep behaviour to have a constant load ($F_{initial} = 16.66\,\mathrm{kN}$) until almost no creep was detected by the clip gauge. This was followed by keeping the crack mouth opening displacement constant with the help of MTS 100 kN 1.3 and the clip gauge. The bolt was screwed into the specimen so that the load on the specimen from the MTS 100 kN 1.3 was transferred solely to the bolt, that is, the bolt was screwed just barely until the load sensors would measure zero load. [15]

2.1.4   Heat treatment

The bolt loaded specimens ($K_I = 30\,\mathrm{MPam}^{1/2}$) were heat treated in $288\,^\circ\mathrm{C}$ for $50\,\mathrm{h}$. This heat treatment results in creep deformation at higher rates due to the elevated temperatures increasing the diffusional properties of dislocations, grains and impurities as explained in §1.1.1. The creep and relaxation of the material will lead to a weaker bolt load. Note that the crack length is constant during the heat treatment. [15]

2.1.5   Measuring bolt tension

The remaining load on the bolt after the creep deformation at the heat treatment stage was measured. The measurement was carried by using the clip gauge to measure the crack mouth opening displacement and using the MTS 100 kN 1.3 to keep the crack mouth opening displacement constant while unscrewing the bolt. When the bolt was fully detached, the force was measured with the load sensor. The remaining force $F_{remaining}$ of the bolt for each sample can be seen in table 2.1.1. [15]

Table 2.1.1. Initial and remaining bolt force $F_{\text{remaining}}$ after heat treatment.

Specimen	F_{initial} [kN]	$F_{\text{remaining}}$ [kN]
1	16.66	12.89
2	16.66	12.93
3	16.66	12.54
4	16.66	12.96
5	16.66	12.83
6	16.66	13.18
7	16.66	13.07
8	16.66	12.79
9	16.66	13.48
10	16.66	13.06
11	16.66	13.49
12	16.66	13.39
13	16.66	12.65

2.2   Rheological models

An uni-axial model for different materials could be made with combinations of simple springs and viscous dash-pots, figure 2.2.1.[6] Models based upon springs and dash-pots are called *rheological models*. Dash-pots are often used to model the viscosity (and plasticity) whereas springs the elasticity of a material.

A spring with the characteristic constant k have a deformation (strain) proportional to the stress

$$\varepsilon = \frac{\sigma}{k} \tag{2.2.1}$$

(a)   (b)
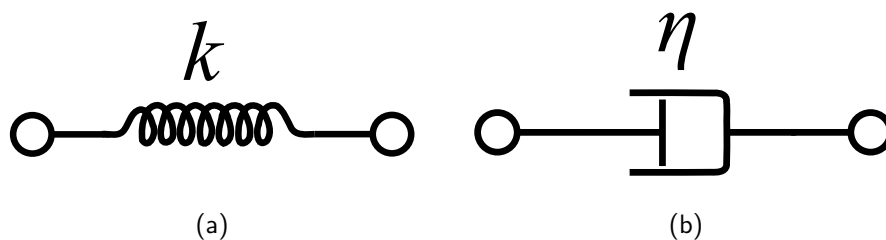
Figure 2.2.1. The rheological components (a) a spring and (b) a dash-pot. (Original source – http://upload.wikimedia.org/wikipedia/commons/d/df/SLS.svg)

which is equivalent to Hooke's law equation (1.2.7) for $k = E$. Therefore, Hooke's law is the most simple rheological model consisting of a spring with characteristic constant equal to the elasticity modulus E.

A dash-pot could be either linear or non-linear. The deformation-rate (strain-rate) of the dash-pot is proportional to the stress,

$$\frac{d\varepsilon}{dt} = B\sigma^m. \tag{2.2.2}$$

If $m = 1$ the dash-pot is linear, otherwise it is considered non-linear. For a linear dash-pot $B = \frac{1}{\eta}$. It can be noted that the dash-pot model was used in equation (1.2.28).

The physical relations to be realised for two components (denoted with indexes 1 and 2) in parallel composition are

$$\sigma_{\text{tot}} = \sigma_1 + \sigma_2 \tag{2.2.3}$$

$$\varepsilon_{\text{tot}} = \varepsilon_1 = \varepsilon_2, \tag{2.2.4}$$

whereas for components in series

$$\sigma_{\text{tot}} = \sigma_1 = \sigma_2 \tag{2.2.5}$$

$$\varepsilon_{\text{tot}} = \varepsilon_1 + \varepsilon_2. \tag{2.2.6}$$

2.2.1   Maxwell model

Consider a linear dash-pot and a spring in series, figure 2.2.2. Notice that the total strain ε_{tot} is given by the sum of the partial strains of the dash-pot and spring according to equation (2.2.6), where ε_1 and ε_2 are the strains of the spring and dash-pot, respectively. Taking the derivative of equation (2.2.6) and substituting the dash-pot strain given by equation (2.2.2) (with $m = 1$) and the derivative of the strain for the spring (with spring constant $k = E$) given by equation (2.2.1) yields

$$\frac{d\varepsilon_{\text{tot}}}{dt} = \frac{1}{E}\frac{d\sigma}{dt} + \frac{\sigma}{\eta}. \tag{2.2.7}$$

Materials that behaves in the manner described by equation (2.2.7) are called to follow the Maxwell model. It is therefore concluded that the model given by equation (1.2.27) is a rheological model given by a dash-pot and spring in series.
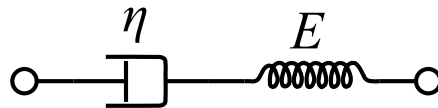
Figure 2.2.2. The rheological Maxwell model. Spring and dash-pot in series. (Original source – http://upload.wikimedia.org/wikipedia/commons/d/df/SLS.svg)
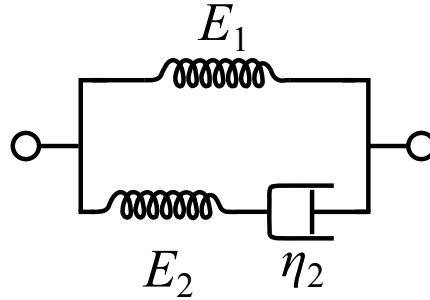
Figure 2.2.3. The rheological SLS-model. A spring in parallel with the Maxwell model. (Original source – http://upload.wikimedia.org/wikipedia/commons/d/df/SLS.svg)

Stress relaxation with the Maxwell model

To find an expression for the stress relaxation with the Maxwell model, the constraint given in equation (1.2.32) is assumed. Hence, equation (2.2.7) is simply the differential equation given by

$$0 = \frac{1}{E}\frac{d\sigma}{dt} + \frac{\sigma}{\eta}. \tag{2.2.8}$$

Solving the differential equation yields

$$\sigma = Ce^{-\frac{E}{\eta}t} \tag{2.2.9}$$

where C is a constant. Further assume that the stress at the time instant $t = 0$ only depends on the spring. Therefore, by recalling equation (2.2.1), finally yields

$$\sigma = E\varepsilon_0 e^{-\frac{E}{\eta}t}. \tag{2.2.10}$$

The constant ε_0 is the spring strain (and therefore also the total strain) at time instant $t = 0$.[6]

2.2.2   Standard linear solid model

The Standard linear solid (SLS) model is also known as the Zener model.[16] It is constituted by a spring in parallel with a Maxwell model. The composition is shown in figure 2.2.3. Recall that the strain in the Maxwell model is given by equation (2.2.7). This strain equals the total strain of the SLS model according to equation (2.2.4). The strain of the parallel spring will also equal the total strain. As given by equation (2.2.3), the total stress of the SLS model is rather the sum of the stress in the Maxwell model, denoted σ_2, and the parallel spring, denoted σ_1. Hence,

$$\sigma_1 = E_1\varepsilon_{\text{tot}} \tag{2.2.11}$$

$$\frac{d\varepsilon_{\text{tot}}}{dt} = \frac{1}{E_2}\frac{d\sigma_2}{dt} + \frac{\sigma_2}{\eta_2}, \tag{2.2.12}$$

where E_1 is the spring constant of the parallel spring. The constants E_2 and η_2 are the spring constant and dash-pot parameter of the Maxwell model, respectively. Substituting equation (2.2.11) into equation (2.2.3) which in turn is substituted into equation (2.2.12) yields the SLS model[16]

$$\frac{d\varepsilon_{\text{tot}}}{dt} = (E_1 + E_2)^{-1}\left(\frac{d\sigma}{dt} + \frac{E_2}{\eta_2}\sigma - \frac{E_1 E_2}{\eta_2}\varepsilon_{\text{tot}}\right), \tag{2.2.13}$$

where $\sigma = \sigma_{\text{tot}}$.

Stress relaxation with the SLS model

The SLS model given by equation (2.2.13) under the constraint given by equation (1.2.32) leads to the linear differential equation of first order

$$\frac{d\sigma}{dt} + \frac{E_2}{\eta_2}\sigma = \frac{E_1 E_2}{\eta_2}\varepsilon_{\text{tot}}. \tag{2.2.14}$$

As the strain is constant according to the contraint given by equation (1.2.32) it is trivial that $\varepsilon_{\text{tot}} = \varepsilon_0$ where ε_0 is the strain at time $t = 0$. The solution to equation (2.2.14) is therefore[17]

$$\sigma = E_1\varepsilon_0 + Ae^{-\frac{E_2}{\eta_2}t}, \tag{2.2.15}$$

where A is a constant to be determined. For the initial condition, assume the material to be elastic and follow Hooke's law given by equation (1.2.7) with elasticity module $E_e = E_1 + E_2$ at time $t = 0$. Hence,

$$A = (E_e - E_1)\varepsilon_0. \tag{2.2.16}$$

Inserting equation (2.2.16) into equation (2.2.15) yields

$$\sigma = E_1\varepsilon_0 + (E_e - E_1)\varepsilon_0 e^{-\frac{E_2}{\eta_2}t} \tag{2.2.17}$$

which describes the stress relaxation using the SLS model.

2.2.3 Generalised Maxwell model

Consider a spring parallel combined with r number of Maxwell models, see figure 2.2.4. Label the parallel added Maxwell models $1, 2, ..., r$, the corresponding strains $\varepsilon_1, \varepsilon_2, ..., \varepsilon_r$ and stresses $\sigma_1, \sigma_2, ..., \sigma_r$. Let also the strain of the single spring be labelled ε_0 and the stress σ_0. Analogously to equation (2.2.4) and equation (2.2.3), the strains for each Maxwell model and the spring are equal

$$\varepsilon_i = \varepsilon_j, \quad \forall i, j \in \{0, ..., r\} \tag{2.2.18}$$

and the total stress is given by the sum of all partial strains

$$\sigma = \sum_{k=0}^{r} \sigma_k. \tag{2.2.19}$$
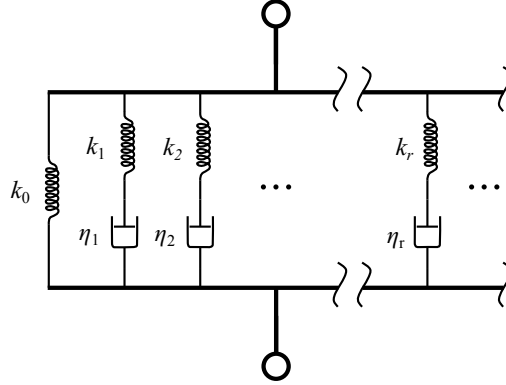
Figure 2.2.4.   The rheological general Maxwell model.   A spring in parallel with several parallel connected Maxwell models.   (Original source – http://upload.wikimedia.org/wikipedia/commons/0/0a/Weichert.svg)

A general differential equation will describe this kind of model and have the form[16]

$$\left(1 + \sum_{k=1}^{p} a_k \frac{d^k}{dt^k}\right) \sigma(t) = \left(m + \sum_{k=1}^{q} b_k \frac{d^k}{dt^k}\right) \varepsilon(t) \tag{2.2.20}$$

with $q = p$ or $q = p + 1$ where p is an integer. The constants m, a_k and b_k are all non-negative. As an example, for $q = p = 1$ having $m = E_1$, $b_1 = \frac{\eta_2}{E_2}(E_1 + E_2)$ and $a_1 = \frac{\eta_2}{E_2}$ gives the SLS model, equation (2.2.13). The Maxwell model given in equation (2.2.7) is given with $q = p = 1$, $b_1 = \eta$ and $a_1 = \frac{\eta}{E}$. Hence, the springs and dash-pots are mainly to give a physical representation of the material behaviour. Equation (2.2.20) is sufficient and covers every possible combination of the springs and dash-pots. For application, a predefinition of the differential order has to be made. Further on, the coefficients a_k and b_k needs to be fitted to experimental data.

If the sought model is of a higher order differential equation given by equation (2.2.20), it is usually convenient to find the solution with the use of Laplace transformation.[16]

Stress relaxation with the generalised Maxwell model

Simply by applying the constraint given in equation (1.2.32) into equation (2.2.20) gives the stress relaxation representative differential equation,

$$\left(1 + \sum_{k=1}^{p} a_k \frac{d^k}{dt^k}\right) \sigma(t) = m\varepsilon_0 \tag{2.2.21}$$

where ε_0 is the instant deformation. The validity of equation (2.2.21) can be verified by comparison with the Maxwell model given by equation (2.2.8) and SLS model given by equation (2.2.14).
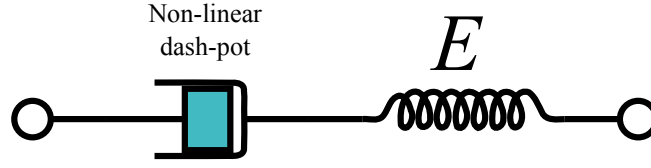
Figure 2.2.5. The rheological Norton model. A spring in parallel with a non-linear dash-pot. (Original source – http://upload.wikimedia.org/wikipedia/commons/d/df/SLS.svg)

2.2.4 Norton model

The Norton creep law follows the behaviour of a non-linear dash-pot, equation (2.2.2). Let a material be described by a linear spring in series with a non-linear dash-pot, seen in figure 2.2.5. Taking the derivative of equation (2.2.6), the total strain rate is given by

$$\frac{d\varepsilon_{\text{tot}}}{dt} = \frac{1}{E}\frac{d\sigma}{dt} + B\sigma^m. \tag{2.2.22}$$

Stress relaxation with the Norton model

To model the stress relaxation at constant strain, equation (1.2.32) and equation (2.2.22) yields

$$\frac{1}{E}\frac{d\sigma}{dt} + B\sigma^m = 0 \quad \Longleftrightarrow \quad \frac{d\sigma}{dt}\sigma^{-m} = -BE. \tag{2.2.23}$$

Integrating both sides with respect to the time t leads to ($m \neq 1$)

$$\sigma^{-m+1} + C = -BEt(-m+1), \tag{2.2.24}$$

where C is a constant to be found with initial conditions. Assume the initial stress, σ_0, at time $t = 0$ is given by the elastic properties of the material. Hence, it is given that $C = -\sigma_0^{-m+1}$. Inserting C into equation (2.2.24), an expression of the stress σ over time is found to be[1]

$$\sigma = \sigma_0 \left(\frac{BEt(m-1)}{\sigma_0^{-m+1}} + 1 \right)^{-\frac{1}{m-1}}. \tag{2.2.25}$$

2.2.5 Bolt relaxation based on Norton's stress relaxation model

Considering equation (2.2.25), equation (1.3.7) and equation (1.3.8), the bolt load can be expressed as

$$F(t) = F_{\text{initial}} \left(\frac{BEt(m-1)}{\sigma_{\text{YS}}^{-m+1}} + 1 \right)^{-\frac{1}{m-1}}, \tag{2.2.26}$$

where the assumption of the initial first order estimate of the plastic zone size (equation (1.3.9)) fully describing the force relaxation has been made. As no creep data for Avesta 308LSi at 288 °C was found, material properties and secondary creep for two fictive

Table 2.2.1. Material data and Norton parameters.

Material	E [Pa]	B	m	σ_{YS}
Fictive material 1	$1.2263 \cdot 10^{11}$	$1.6059 \cdot 10^{-28}$	2.234	$90.1 \cdot 10^{6}$
Fictive material 2	$1.93 \cdot 10^{11}$	$5 \cdot 10^{-48}$	5	$2.1 \cdot 10^{8}$

material data were used, shown in table 2.2.1. The elasticity module and yield strengths of Fictive material 1 and Fictive material 2 are typical values for stainless steel at $550\,^{\circ}C$ and at room temperature, respectively.[18,19] The Norton's creep parameters B and m for Fictive material 1 are somewhat near a real case creep behaviour, but not statistically significant.[19] The Norton parameters for Fictive material 2 are chosen in such a way to yield a larger creep deformation compared to Fictive material 1 during the transient. This is to highlight different effects that might occur in materials with large creep deformations compared to low creep deformations.

Only the Norton model, equation (2.2.22), was modelled with the creep parameters B and m. It is a general version of the Maxwell model (noticed by comparison of §2.2.1 and §2.2.4), thus the Maxwell model is discarded. The other creep models presented in §1.2.3 require real data points for curve fitting to yield realistic behaviours. As real data points are not available, these are discarded. For example, the general Maxwell model could become a more advanced creep model than the Norton model when consisting of enough number of parameters, although the large number of parameters needed makes it a tedious choice. Also note that the SLS model is the simplest case of the general Maxwell model. The main difference between the SLS stress relaxation model and the Norton stress relaxation model is the exponential declining versus inverse power function behaviour. For long term behaviours it is given that according to the Norton stress relaxation model the stresses tend to zero, while the SLS stress relaxation model the stress tend to a fix value. By assuming that the material is relaxing until reaching zero stress in elevated temperatures $(288\,^{\circ}C)$, the Norton model is the only reasonable candidate for modelling the stress relaxation.

The load relaxation model (equation (2.2.26)), derived from Norton's stress relaxation model, for Fictive material 1 and Fictive material 2 (given in table 2.2.1) can be seen in figure 2.2.6(a) and figure 2.2.6(b). The parameters for fictive material 1 was chosen to produce a slower relaxation compared to experimental data (table 2.1.1) and, in contrast, the fictive material 2 has a faster relaxation.
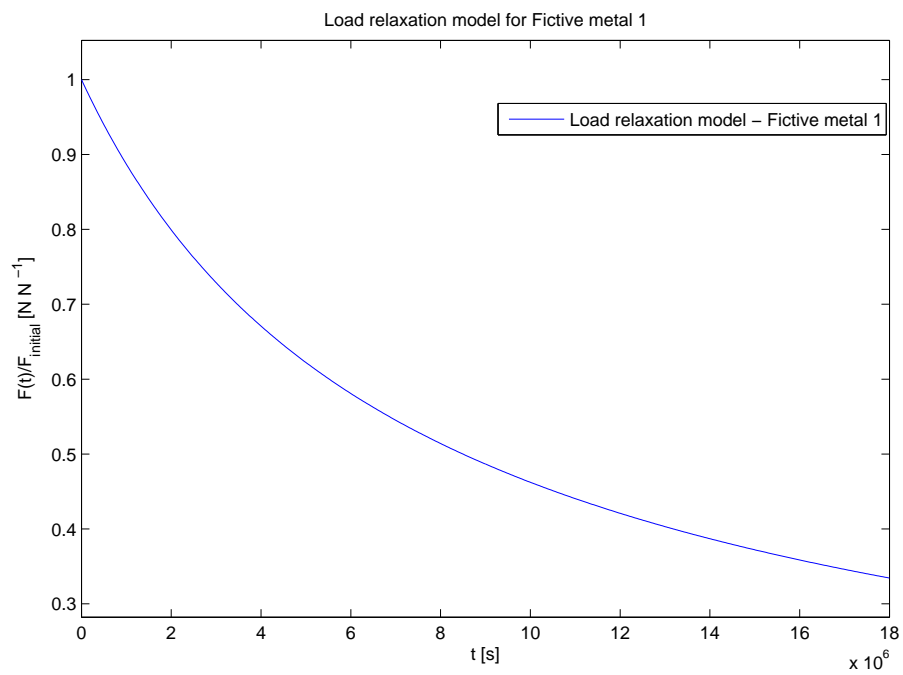
(a)
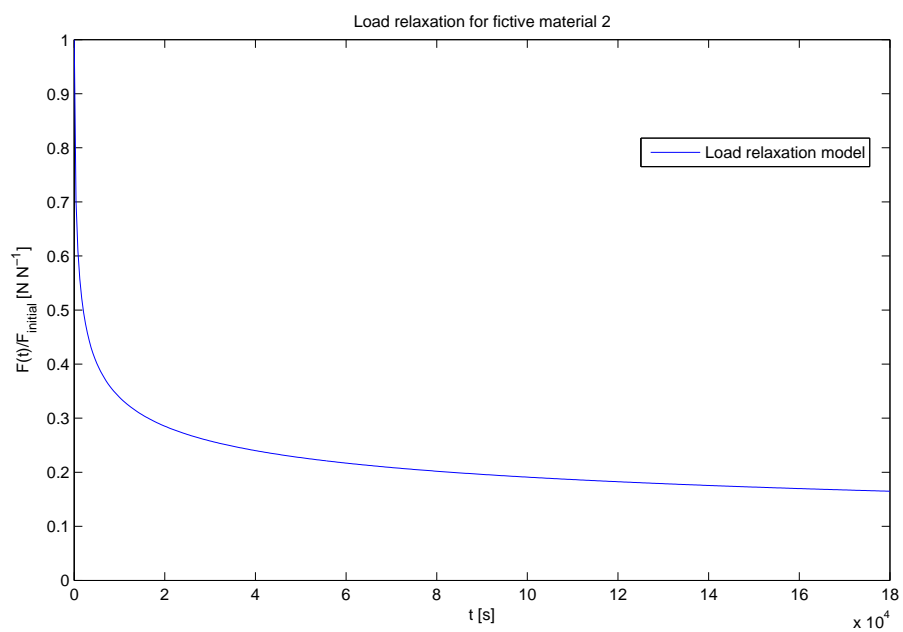
(b)

Figure 2.2.6. The load relaxation of (a) Fictive material 1 and (b) Fictive material 2.

I am deathless, I am the eternal Lord
For I have spread the seed of the Word.

– Abolqasem Ferdowsi

Results

This chapter is subdivided into individual sections concerning comparison of the theoretical and FEM-calculation results.

3.1 Numerical analysis using Ansys

The numerical FEM analysis performed with the software tool called Ansys. The software has tools not only for FEM calculations but also for Computer-aided design (CAD). The CAD tool is used to create a solid model of the specimen used in the heat transient. The bolt was also included in the design to simulate the experiment as close to the reality as possible.

3.1.1 Geometry

The CT-specimen was designed in accordance to the drawing 3003329 Revision 2 shown in appendix A, and the bolt according to 1090900 Revision 03 (drawing given in appendix B). The internal threads and external threads were omitted in the design to reduce calculation time. Due to the meshing, the threads would yield enormous amount of small elements. The absence of the threads are assumed to not affect the stress in front of the crack tip as the threads are far away from that region. A threaded bolt and CT-specimen can be seen in figure 3.1.1(a) and figure 3.1.1(c), respectively. Their corresponding non threaded geometries used for the numerical FEM-calculations can be seen in figure 3.1.1(b) for the bolt and figure 3.1.1(d) for the CT-specimen. The assembled bolt and CT-specimen can be seen in figure 3.1.2.

3.1.2 Input data

Considering the material properties of the bolt and CT-specimen, calculations for four different cases were performed. The cases are explained below,

1. The entire assembled geometry's material was assumed to be linear-elastic (following Hooke's law, §1.2.1) to calculate the stress intensity factor (with Ansys built-in calculation tool for stress intensity factors) and compare it to theoretical results. This was performed to verify the numerical FEM-model and design of the geometry.
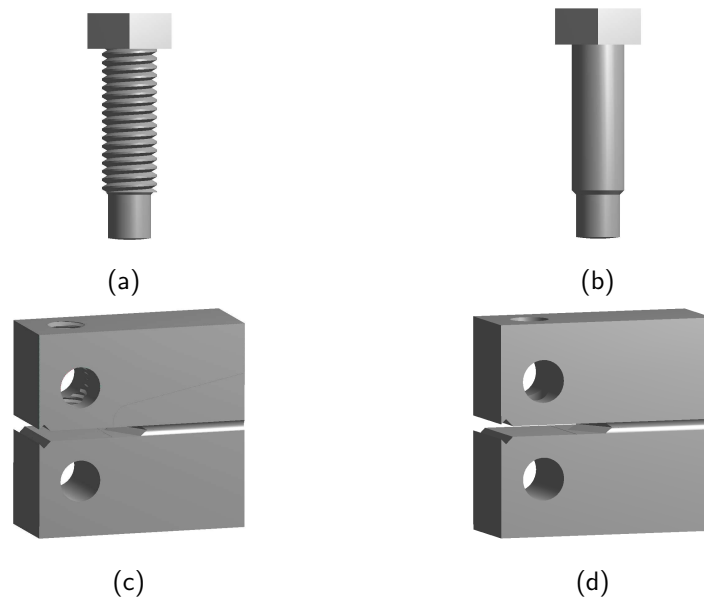
Figure 3.1.1. The designed solid geometries of (a) the threaded bolt and (b) the corresponding non threaded bolt, as well as the geometry of (c) the threaded CT-specimen and (d) the corresponding non threaded CT-specimen. The non threaded geometries were used for numerical FEM-calculations.

2. The material of the bolt is still assumed to be linear-elastic, but the CT-specimen is non-linear following a bilinear stress–strain relationship (the slope of the line at the plastic region is denoted E_b) and Norton's creep law. Norton's creep law is the most common creep law behaviour in the literature.[1,6] The creep law parameters are fictive.

3. Similar to 2 but with other material and creep law parameters corresponding to Fictive material 1.

4. Both the bolt and CT-specimen are assumed to follow a bilinear stress-strain relationship. They are both assumed to follow the material parameters of Fictive material 1. Both the bolt and CT-specimen follow Norton's creep law. The Norton's creep law was chosen to be able verify the theoretical load relaxation (which is based on the Norton's creep law) with the numerical FEM-calculation results.

Table 3.1.1 and table 3.1.2 summarise the material and Norton creep parameters for the bolt and CT-specimen in each case. The cases were chosen to show different aspects of the impact of the bolt material being prone to creep deformation or not. This is indeed due to the fact that the bolt have an impact on the remaining bolt tension if being prone to creep behaviours or not. The elasticity module and yield strength differs for higher temperatures and therefore the material parameters for two of the cases are chosen to follow material parameters for stainless steel at $550\,^\circ C$. Hence the different cases covers
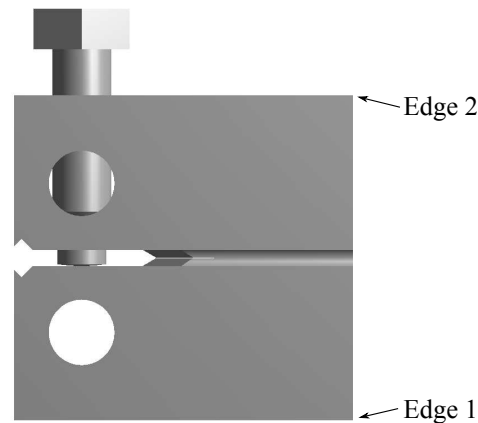
Figure 3.1.2. The assembled bolt and CT-specimen.

Table 3.1.1. Input data and Norton parameters for the bolt at different cases.

Case	E [Pa]	ν	σ_{YS} [Pa]	E_b [Pa]	B	m
1	$1.93 \cdot 10^{11}$	0.31	N/A	N/A	N/A	N/A
2	$1.93 \cdot 10^{11}$	0.31	N/A	N/A	N/A	N/A
3	$1.2263 \cdot 10^{11}$	0.31	N/A	N/A	N/A	N/A
4	$1.2263 \cdot 10^{11}$	0.31	$90.1 \cdot 10^6$	$1.8 \cdot 10^9$	$1.6059 \cdot 10^{-28}$	2.234

the effects caused by the bolt material being prone creep behaviour or not and also the effects of the material behaviours following typical stainless steel at elevated temperatures.

3.1.3   Meshing

The meshing was generated by taking into account the requirement for higher accuracy around the crack tip. The mesh for the entire CT-specimen is shown in figure 3.1.3. Bearing this in mind, smaller elements were produced around the crack tip. To manage the calculations in a reasonable amount of time (around 4 h) with the computing power at hand, the elements were designed and aligned as favourably mentioned in §1.4.1 to reduce the amount needed to be generated. The generated mesh around the crack tip can be seen in figure 3.1.4.

Defining contact surfaces

In Ansys, the surfaces where the two bodies (the bolt and CT-specimen) are in contact, needs to be defined. The contacts definitions between the bolt and the CT-specimen are set where they are threaded as well as at the bottom of the bolt. The type of contact

Table 3.1.2. Input data and Norton parameters for the CT-specimen at different cases.

Case	E [Pa]	ν	σ_{YS} [Pa]	E_b [Pa]	B	m
1	$1.93 \cdot 10^{11}$	0.31	N/A	N/A	N/A	N/A
2	$1.93 \cdot 10^{11}$	0.31	$2.1 \cdot 10^8$	$1.8 \cdot 10^9$	$5 \cdot 10^{-48}$	5
3	$1.2263 \cdot 10^{11}$	0.31	$90.1 \cdot 10^6$	$1.8 \cdot 10^9$	$1.6059 \cdot 10^{-28}$	2.234
4	$1.2263 \cdot 10^{11}$	0.31	$90.1 \cdot 10^6$	$1.8 \cdot 10^9$	$1.6059 \cdot 10^{-28}$	2.234
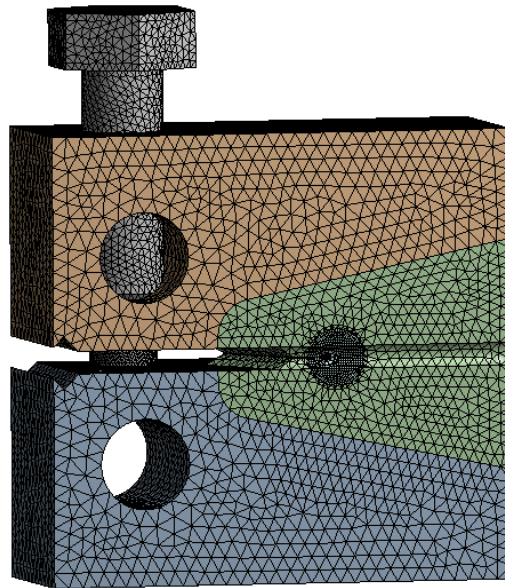
Figure 3.1.3. Smaller mesh elements in front of the crack tip.

is defined to be *bonded* as it is assumed the surfaces in contact won't move relative to each other during the transient. The contact definition at the bottom of the bolt has also a pinball region defined to help Ansys easier detect the contact at that region during the transient. This was set due to the entire surface of the bolt end not being in contact with the CT-specimen in the beginning of the transient.

3.1.4 Bolt pretension

The bolt force was defined with the bolt pretension tool. It was selected at the bottom cylinder of the bolt. The pretension tool could be briefly explained as cutting the cylinder into two bodies by making the stiffness of the elements along the cut surface to zero and thereafter pushing then away from each other along shared symmetry axis. The deformation is performed until the reaction forces of each of the two bodies reaches a
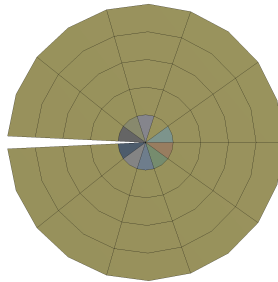
Figure 3.1.4. The meshed elements in front of the crack tip.

predefined force value. Hence, the bolt pretension tool was set to reach a reaction force of $-16{,}66\,\mathrm{kN}$ where the minus sign denotes the separation of the two bodies. The bolt pretension tool does not simulate the real case of screwing the bolt to a certain load but is assumed to not have an impact on the results of the stress near the crack tip as it is spatially far away from that region. To make sure the solution converges, fixed displacements are also defined. The concerned edges (edge 1 and edge 2) are shown in figure 3.1.2. Edge 1 is fixed in all spatial directions while edge 2 is only constrained along the crack front propagation direction.

3.1.5 Ansys results

The stresses along with exaggerated deformation results for case 1 can be seen in figure 3.1.5(a) and the true deformation in figure 3.1.5(b). The Stress intensity factor along the crack edge is shown in figure 3.1.6 for case 1. It can be noted that it follows the theoretical results (around $30\,\mathrm{MPam}^{1/2}$ with a $16.66\,\mathrm{kN}$ bolt tension). At both ends of the crack edge the stress intensity factor is extremely large. This is probably where the three dimensional effects of the stress distributions makes a difference compared to the centre of the crack edge. Another reason for the distinction occurring at both ends of the crack edge could be due to the circular shaped side grooves redistributing the stresses at the sides of the crack edge differently than in the centre of the crack edge.

The stress and deformation results for case 2 at the end of the bolt pretension and after the heat transient can be seen in figure 3.1.7. Zoomed results of the crack tip shape are also included. As can be noticed in the zoomed in crack tips, during the transient the crack tip is blunting. Additionally, the stress relaxation effect is clearly shown.

The results for case 3 and case 4 are seen in figure 3.1.8 and figure 3.1.9, respectively, but without any crack tip blunting occurrence. Almost no stress relaxation could be observed.

B: Static Structural
Equivalent Stress
Type: Equivalent (von-Mises) Stress
Unit: Pa
Time: 180000
2014-04-17 12:23

1,9175e9 Max
7e8
6,4615e8
5,9231e8
5,3846e8
4,8462e8
4,3077e8
3,7692e8
3,2308e8
2,6923e8
2,1538e8
1,6154e8
1,0769e8
5,3847e7
496,1 Min

(a)

B: Static Structural
Equivalent Stress
Type: Equivalent (von-Mises) Stress
Unit: Pa
Time: 180000
2014-04-17 12:25

1,9175e9 Max
7e8
6,4615e8
5,9231e8
5,3846e8
4,8462e8
4,3077e8
3,7692e8
3,2308e8
2,6923e8
2,1538e8
1,6154e8
1,0769e8
5,3847e7
496,1 Min

(b)

Figure 3.1.5. The stresses and (a) exaggerated deformations as well as (b) the true deformation of the CT-specimen. Results carried with the use of Ansys on material data of case 1.
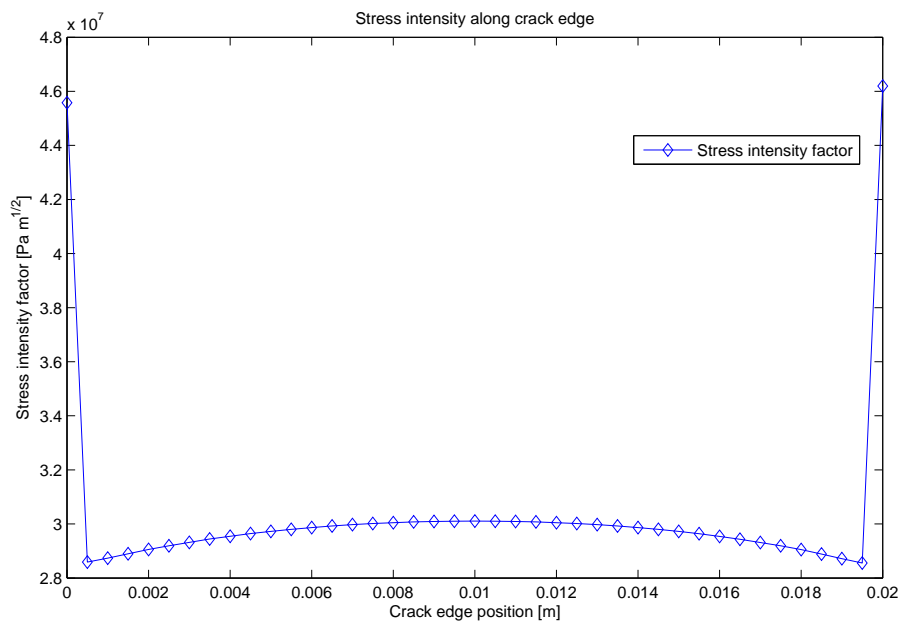
Figure 3.1.6. Stress intensity factor along the crack edge for case 1.

(a)

(b)

(c)

(d)
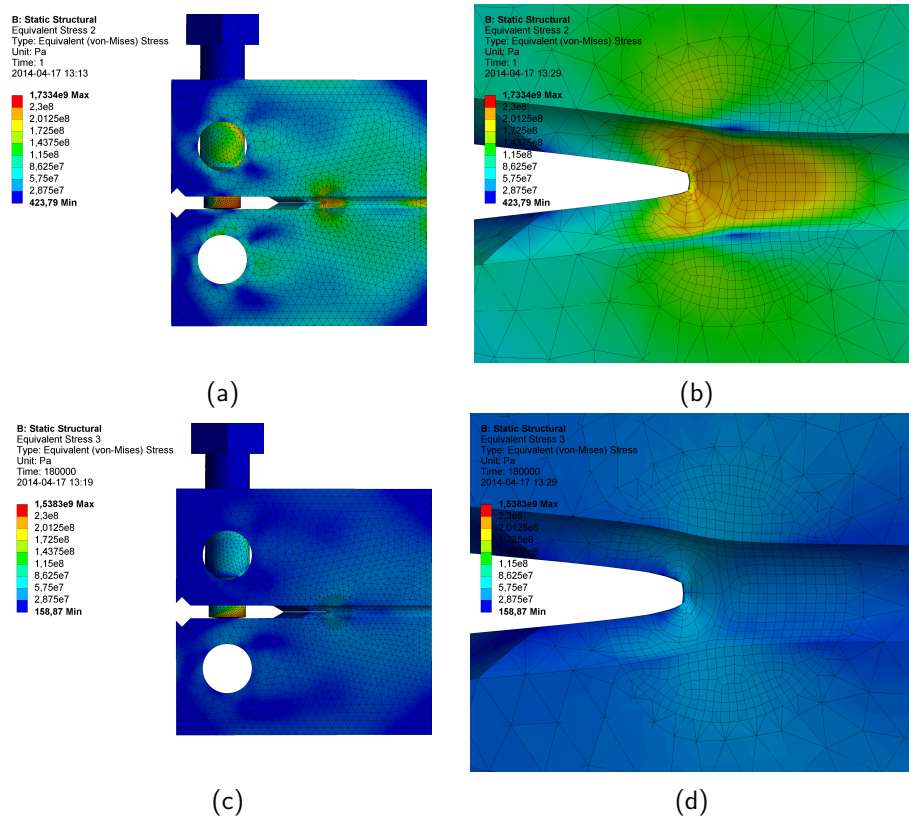
Figure 3.1.7. The stress and deformation with case 2 parameters for (a) the initial state of the CT-specimen and (b) a zoomed picture of the crack tip. The corresponding results at the end of the transient for (c) the CT-specimen and (d) the zoomed in crack tip.

(a)   (b)

(c)   (d)
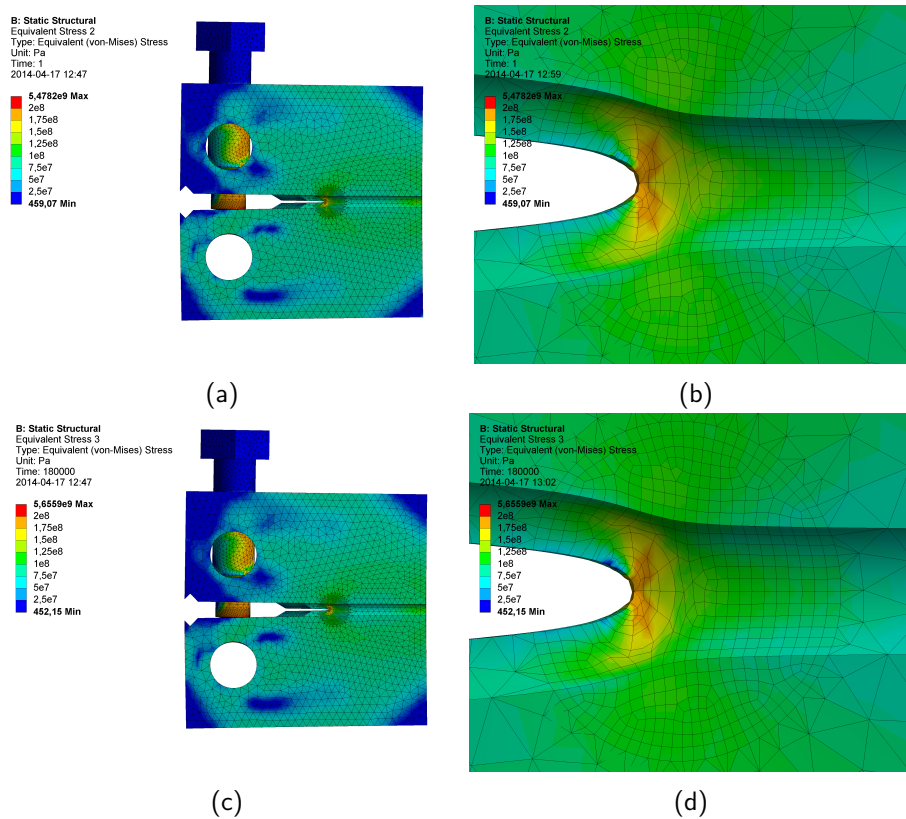
Figure 3.1.8. The stress and deformation with case 3 parameters for (a) the initial state of the CT-specimen and (b) a zoomed picture of the crack tip. The corresponding results at the end of the transient for (c) the CT-specimen and (d) the zoomed in crack tip.

(a)   (b)
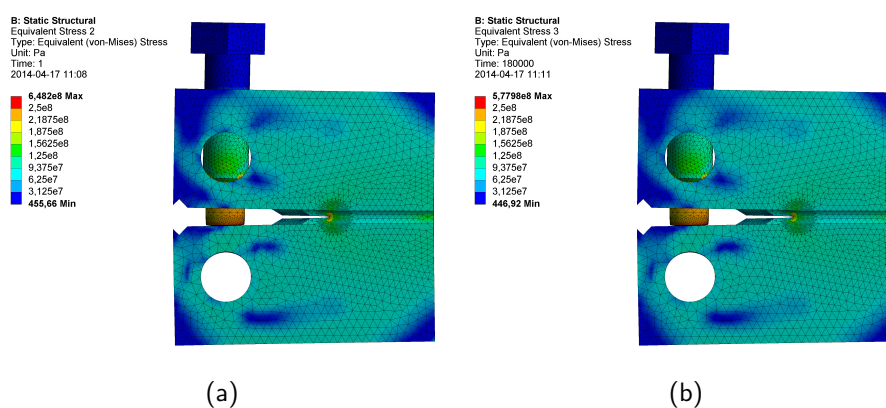
Figure 3.1.9. The stress and deformation with case 4 parameters for (a) the initial state of the CT-specimen and (b) at the end of the transient for the CT-specimen.

3.2   Comparison of theoretical models to numerical FEM calculation results

The remaining bolt load of the numerical FEM-calculation results together with the theoretical bolt load relaxation model for case 3 and case 4 are shown in figure 3.2.1. The bolt load relaxation model and the Ansys bolt load results during the transient for case 2 is given by figure 3.2.2. For case 2, the rate of change of the bolt load from the FEM-calculation results compared to the relaxation model are almost equal at the end of the transient.
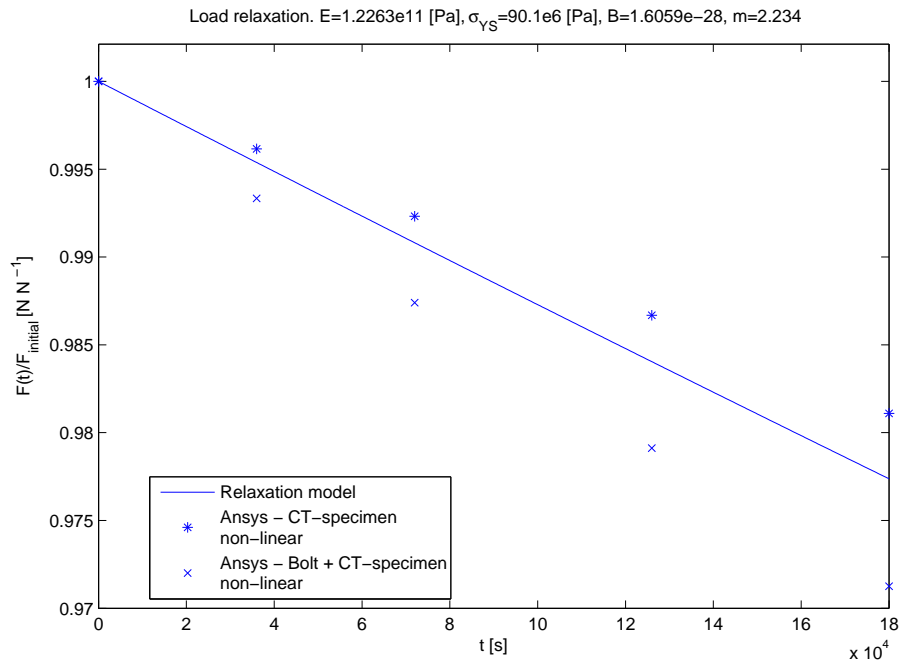
Figure 3.2.1. Theoretical bolt load relaxation model (with CT-specimen parameters for case 3 and case 4) and the Ansys case 3 and case 4 results.
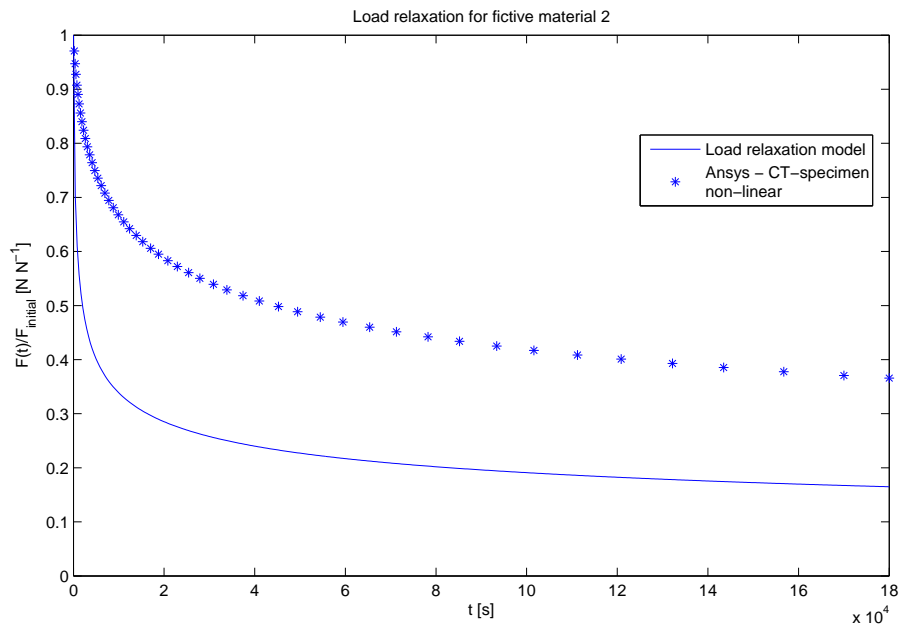
Figure 3.2.2. Theoretical bolt load relaxation model (with CT-specimen parameters for case 2) and the Ansys case 2 results.

Conclusions

With Norton's creep model, it has been shown that the bolt tension can be fairly well estimated during the transient compared to the numerical FEM-calculation performed. Although, this is of no worth if the experimental results won't show a similar behaviour. Hence for verification, further experiments are required, see §4.3.

The relaxation model could be calibrated if needed to fit the numerical FEM-calculation results. Preferably by increasing or decreasing σ_{YS} by a factor to minimise the error for a particular load and material case.

The long term effects of the numerical FEM-calculated (and experimental) bolt load relaxation rate is well described by the relaxation model.

One concern of the model and numerical FEM-calculations are the assumptions of constant temperature. During the heat transient (elevation of the temperature from room temperature to $288\,^{\circ}C$) the material expands. The expansion of the material might affect the initial stresses, that is, increasing or decreasing the magnitude of the forces while have reached the desired temperature. The expansion effect on the initial stresses was discarded as it could be assumed that larger or smaller bolt loads were initially applied to the specimen. The shape of the bolt load relaxation curves would still be similar to the achieved results. The expansion effect changes the geometrical values of the specimen (effecting the theoretical value of the stress intensity factor). The geometrical changes of the specimen were also discarded, assuming the changes were negligible.

4.1   Remarks about the theoretical results

The theoretical bolt load relaxation model is derived by linear elastic material assumptions. The stresses being proportional to the stress intensity factor is only valid far away from the crack tip. If large creep rates are present, the assumptions made during the derivation of the bolt load relaxation could result in an inaccurate model. The stress intensity factor for a CT-specimen assumes sharp crack tips and does not take the crack blunting into account. Although, due to the stresses decreasing with an increased radius of crack tip curvature, for conservative safety verifications this is not to be of any concern. This is explained by the linear elastic case brings a harsher crack tip state than the ductile/plastic/non-linear case.

It can be noted that neither the Fictive material 1 nor Fictive material 2 has similar decreases in bolt load relaxation as to the experimental results carried on by KTH, most probably due to the creep parameters not corresponding to the material used.

An additional assumption that could be questioned, due to the lack of verification with experimental results, is the models eligibility due to the first order estimation of the initial plastic zone size. It is not verified if that is the best position in front of the crack tip where the stress is explaining the relaxation.

No reversible creep effects has been taken into account after the transient.

For all assumptions to be verified and eligible, additional experiments are required.

4.2 Remarks about the numerical FEM-calculation results

The performed numerical FEM-calculation results of the linear elastic case are coherent with the theory. The stress intensity factor yield similar results to the theory, thus the model in Ansys are likely to be correct. The crack tip is simply sharp enough for the material used after the load being applied. Even though the results in this matter seems satisfactory, they have to be verified for each material used.

The material and settings according to case 2 show a large plasticity in front of the crack tip. The stresses in the plastic zone decrease as the material relaxes as expected. Interestingly, the crack tip starts to blunt during the relaxation. Thus, the strain is not constant. The blunting is affecting the stresses in front of the crack tip in such a way that an increase in the crack tip curvature radius decreases the stresses further along with the decrease of stresses only due to the stress relaxation. If a conservative model is to be used for modelling the stresses in front of the crack tip, the blunting is not of any concern.

In case 3 (and case 4), no crack tip blunting could be observed. This is most likely due to the low creep rates for that particular case.

4.3 Future work

The lack of experimental creep results for different stresses at different temperatures for Avesta 308LSi brought the biggest challenges to this report. Therefore, an uni-axial stress relaxation or creep deformation experiment is highly recommended for all materials used in the interested temperature regime. This also applies for the bolt material. The results of such experiment could be used to curve fit the various creep models presented in this report. Further on, the use these creep models in the numerical FEM analysis to verify the validity in the three dimensional case for the CT-specimen should thereby be done. By verifying the numerical FEM-calculation results with the already performed experimental bolt relaxation results, the material creep behaviour in the CT-specimen could be assumed to be completely described.

For further validity, it is largely recommended to measure the bolt load with certain time intervals during the experimental transient compared to *only* the initial and remaining bolt load after the experimental transient. Perhaps the measurements could be made at

every $5\,h$ (to extract additional 9 data points during the $50\,h$ transient) to enable the possibility to verify the shape of the bolt relaxation model.

To not have to concern about the bolt material relaxing and thereby affecting the experimental results, choose the bolt material with care that have significantly lower creep rates than the weld material inside the CT-specimen at the temperatures of the transient/heat treatment cycle.

Verification and comparison of the analytical bolt load relaxation model derived from the Norton model with the other models presented could be beneficial.

Bibliography

[1] Anderson TL. *Fracture Mechanics – Fundamentals and Applications.* 2nd ed. Boca Raton (FL): CRC Press; 1994.

[2] ASTM Standard E647-13a. *Standard Test Method for Measurement of Fatigue Crack Growth Rates.* West Conshohocken (PA): ASTM International; 2013. DOI: 10.1520/E0647.

[3] ASTM Standard E1820-13. *Standard Test Method for Measurement of Fracture Toughness.* West Conshohocken (PA): ASTM International; 2013. DOI: 10.1520/E1820.

[4] Carlsson J. *Brottmekanik.* Stockholm (Sweden): Ingenjörsförlaget; 1976. Swedish.

[5] Nilsson F. *Fracture Mechanics – from Theory to Application.* Stockholm (Sweden): Department of Solid Mechanics, KTH; 2001.

[6] Dowling NE. *Mechanical Behavior of Materials.* 4th ed. Harlow (United Kingdom): Pearson Education; 2012.

[7] Jenssen A, Engman U. *Lastrelaxation i bultbelastade CT- och WOL-prov – Sammanställning av erfarenheter från genomförda provningar.* Nyköping (Sweden): Studsvik Nuclear AB; 2010. Studsvik/N-10/142. Swedish.

[8] Kittel C. *Introduction to Solid State Physics.* 8th ed. Hoboken (NJ): John Wiley & Sons; 2004.

[9] Robinett RW. *Quantum Mechanics – Classical Results, Modern Systems, and Visualized Examples.* 2nd ed. Oxford (NY): Oxford University Press; 2006.

[10] Lundh H. *Grundläggande hållfasthetslära.* Stockholm (Sweden): Department of Solid Mechanics, KTH; 1994. Swedish.

[11] Lapidus L, Pinder GF. *Numerical Solution of Partial Differential Equations in Science and Engineering.* New York: John Wiley and Sons; 1982.

[12] Zienkiewics OC, Taylor RL. *The Finite Element Method.* 4th ed. New York: McGraw-Hill; 1989.

[13] Rizzo FJ. An Integral Equation Approach to Boundary Value Problems of Classcal Elastostatics. *Quarterly of Applied Mathematics.* 1967;**25**:83–95.

[14] Finch RF. *Performance welding.* Osceola (WI): MBI; 1997.

[15] Anttonen JP, Åström B. *Tillverkning av testblock för CT-provstavar.* Stockholm (Sweden): Swerea KIMAB; 2011. Report no. 658010. Swedish.

[16] Mainardi F, Spada G. Creep, Relaxation and Viscosity Properties for Basic Fractional Models in Rheology. *The European Physical Journal, Special Topics.* 2011;**193**:133–160.

[17] Råde L, Westergren B. *Mathematics Handbook for Science and Engineering.* 5th ed. Lund (Sweden): Studentlitteratur; 2004.

[18] ASM Aerospace Specification Metals, Inc [homepage on the Internet]. Pompano Beach (FL): ASM Aerospace Specification Metals, Inc; [cited 2014 Mar 27]. AISI Type 304L Stainless Steel. Available from: `http://asm.matweb.com/search/SpecificMaterial.asp?bassnum=MQ304L`.

[19] Hayhurst DR, Vakili-Tahami F, Zhou JQ. Constitutive equations for time independent plasticity and creep of 316 stainless steel at 550 °C. *The International Journal of Pressure Vessels and Piping.* 2003 Feb;**80**(2):97–109.

Appendices

Drawing 3003329 Revision 2

CLASSIFIED

Drawing 1090900 Revision 03

CLASSIFIED